


Review

# Recent Progress on Supramolecular Luminescent Assemblies Based on Auophilic Interactions in Solution

Guillermo Romo-Islas<sup>1</sup> and Raquel Gavara<sup>2,\*</sup> 

<sup>1</sup> Departamento de Química Inorgánica i Orgànica, Secció de Química Inorgànica, Universitat de Barcelona, Martí i Franquès 1-11, E-08028 Barcelona, Spain; guillermo.romo@qi.ub.es

<sup>2</sup> Departamento de Química Inorgánica, Universidad Autónoma de Madrid, 28049 Madrid, Spain

\* Correspondence: raquel.gavara@uam.es

**Abstract:** The development of supramolecular systems showing auophilic interactions in solution is gaining much attention in the last years. This is due to the intriguing photophysical properties of gold(I) complexes, which usually confer to these supramolecular assemblies interesting luminescent properties, as well as the possibility of morphological modulation, through fine tuning of inter- and intramolecular auophilic interactions, in synergy with the formation of other supramolecular contacts. In this work, an overview of the advances made in this area since 2015 is presented. A large variety of systems showing different spectroscopical and structural topologies has been reported. Moreover, these supramolecular assemblies have proven to be useful in a wide range of applications.

**Keywords:** gold(I) complexes; aggregation-induced emission; self-assembly; metallogelators; luminescent chemosensors; self-assembly modulation by cations and anions



**Citation:** Romo-Islas, G.; Gavara, R. Recent Progress on Supramolecular Luminescent Assemblies Based on Auophilic Interactions in Solution. *Inorganics* **2021**, *9*, 32. <https://doi.org/10.3390/inorganics9050032>

Academic Editor: Claudio Pettinari

Received: 14 March 2021

Accepted: 13 April 2021

Published: 22 April 2021

**Publisher's Note:** MDPI stays neutral with regard to jurisdictional claims in published maps and institutional affiliations.



**Copyright:** © 2021 by the authors. Licensee MDPI, Basel, Switzerland. This article is an open access article distributed under the terms and conditions of the Creative Commons Attribution (CC BY) license (<https://creativecommons.org/licenses/by/4.0/>).

## 1. Introduction

Gold(I) complexes have attracted much attention over the past decades due to their ability to assemble through auophilic interactions [1–3]. This kind of non-covalent force is present when two gold(I) ions are separated by a distance which is shorter than the sum of their van der Waals radii (ca. 3.6 Å), which is usually found in the range 2.8–3.5 Å. Auophilic interactions are a consequence of the strong relativistic effects affecting the closed-shell (5d<sup>10</sup>) configuration of gold(I) ions and are classified as one of the strongest supramolecular forces that can be found in Chemistry. In fact, their strength (20–50 kJ mol<sup>−1</sup>) can be comparable to that shown by strong hydrogen bonds [4]. Additionally, gold(I) complexes usually exhibit interesting luminescent properties, which arise from the heavy atom effect of gold that favors the intersystem crossing and facilitates the emission from low-lying triplet states. Interestingly, this emission can be modulated by the establishment of Au(I)⋯Au(I) interactions, giving rise to supramolecular assemblies and aggregating with new emissive properties [5–9].

Traditionally, gold(I)-gold(I) interactions have been detected in crystal structures of gold(I) complexes as a critical supramolecular motif that allows the assembly in the solid state. This fact has been exploited by scientists to develop systems with response to different external stimuli, arising from the observation that the application of an external stimuli produces changes in the auophilic contacts, that in turn drastically affects to the luminescence exhibited by the materials. Using this strategy, a high number of vapo-chromic, solvatochromic, thermochromic and mechanochromic solids have been developed [5,10–12].

Interestingly, the number of examples reporting auophilic contacts in solution is exponentially growing in the last years. It has been observed that the presence of Au(I)⋯Au(I) contacts modulates the luminescence of the aggregates observed in solution, giving rise to aggregation-induced emission luminogens [7]. Moreover, the establishment of these interactions together with other supramolecular forces, such as hydrogen bonding or π-π

stacking, has originated new soft supramolecular assemblies—for example, metallogelators, that present new functional properties not exhibited by the original compounds [13]. Finally, aurophilic interactions can be also modulated intramolecularly, originating new luminescent molecules for which emission can be tuned by interaction with other species in solution. This behavior has been proven to be useful in the preparation of new luminescent probes and chemosensors [6,8,14].

The present review focuses on the recent developments (since 2015) on luminescent supramolecular assemblies in solution, where aurophilic interactions play a key role. The work is divided into three main sections: (i) luminescent gold(I) clusters; (ii) self-assembly of gold(I) complexes; and (iii) modulation of gold(I) supramolecular assemblies based on the interaction with other species. Heterometallic complexes as well as clusters where gold atoms present a mixed valence (0/I) are out of the scope of the present review. Every section includes the description of the gold(I) systems as well as their potential application in different fields.

## 2. Gold(I) Clusters as Discrete Luminescent Units

Aurophilic interactions play an important role on the supporting of self-assembled gold(I) clusters and confer interesting luminescent properties to these gold(I) polynuclear species [8,15,16]. During the last years, several gold(I) clusters showing luminescent properties in solution have been reported. Thus, in 2015, Yu, Jiang et. al described the self-assembly of gold(I) centers to produce a polynuclear supramolecular structure containing sixteen gold(I) ions [17]. The authors prepared the tetramer  $\{[\text{Au}_4(\mu\text{-dppm})_2(\mu\text{-dctp}^{2-})]^{2+}\}_4$  (dppm = bis(diphenylphosphino)methane,  $\text{dctp}^{2-} = N,N'$ -bis(dicarbodithioate)-2,11-diaza[3.3]paracyclophane) (**1**, Figure 1), by reaction between the dicarbodithioate ligand and  $(\text{dppm})\text{Au}_2\text{Cl}_2$  in methanol and precipitated it with an excess of  $\text{NaBF}_4$ . Aurophilic interactions, with  $\text{Au}^I \cdots \text{Au}^I$  average distances of 2.949 Å, were revealed by single-crystal X-ray analysis of the compound, which exhibited yellow phosphorescence in deoxygenated acetonitrile solutions. The broad emission band, centered at 500 nm, was tentatively assigned to be originated from triplet-excited states of metal centers (ds/dp) and ligand-to-metal charge transfer character was modified by aurophilic interactions.

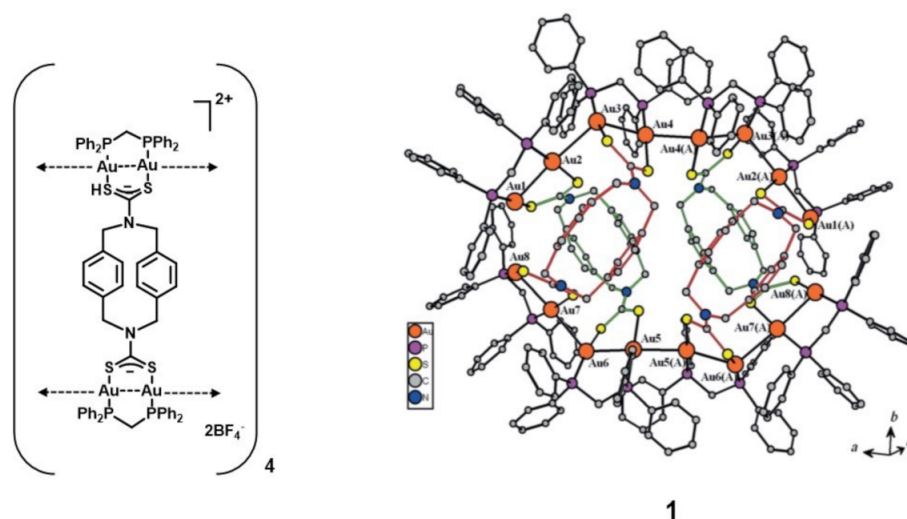


**Figure 1.** Left: Chemical structure of the tetramer **1** self-assembled by means of aurophilic interactions. Right: X-ray structure of the compound obtained from crystals grown in  $\text{CH}_3\text{CN}$ . 8  $\text{BF}_4^-$  units are placed outside the cationic macrocycle. H atoms are omitted (gold-Au, yellow-S, purple-P, gray-C, blue-N). Adapted with permission from ref. [17]. Copyright 2015 John Wiley and Sons.

In 2016, Yam et al. reported the preparation of several chiral sulfido clusters by employing the chiral precursors R- or S-[BINAP( $\text{AuCl}$ ) $_2$ ] [18] (Figure 2). Reaction of



the respective precursors with  $\text{H}_2\text{S}$  rendered the decanuclear clusters **2(R)** and **2(S)**. The compounds were supported by aurophilic interactions as demonstrated by single crystal X-ray analysis ( $\text{Au}^{\text{I}}\cdots\text{Au}^{\text{I}}$  contacts between ca. 3.0 and 3.3 Å) and displayed a structured and long-lived  $^3\text{IL}$  luminescence centered at ca. 550 nm in dichloromethane. Hexanuclear clusters **3(R)** and **3(S)** were isolated using  $\text{Li}_2\text{S}$  instead of  $\text{H}_2\text{S}$  as a sulfide source with a stoichiometry 1:3 with respect to the chiral precursors. For these compounds, single crystal X-ray analysis revealed  $\text{Au}^{\text{I}}\cdots\text{Au}^{\text{I}}$  distances comprised between 3.0 and 3.2 Å, approximately. The clusters exhibited a similar although unstructured emission centered at 550 nm in solution. Additionally, all the chiral clusters displayed an intense Cotton effect in the corresponding circular dichroism (CD) spectra with a mirror image relationship between the enantiomers in the range of 250–380 nm. Interestingly, the racemic mixture of **2(R)** and **2(S)** underwent a rearrangement and heterochiral self-sorting, giving rise to a meso decanuclear cluster which did not show either CD signal nor luminescence in solution.

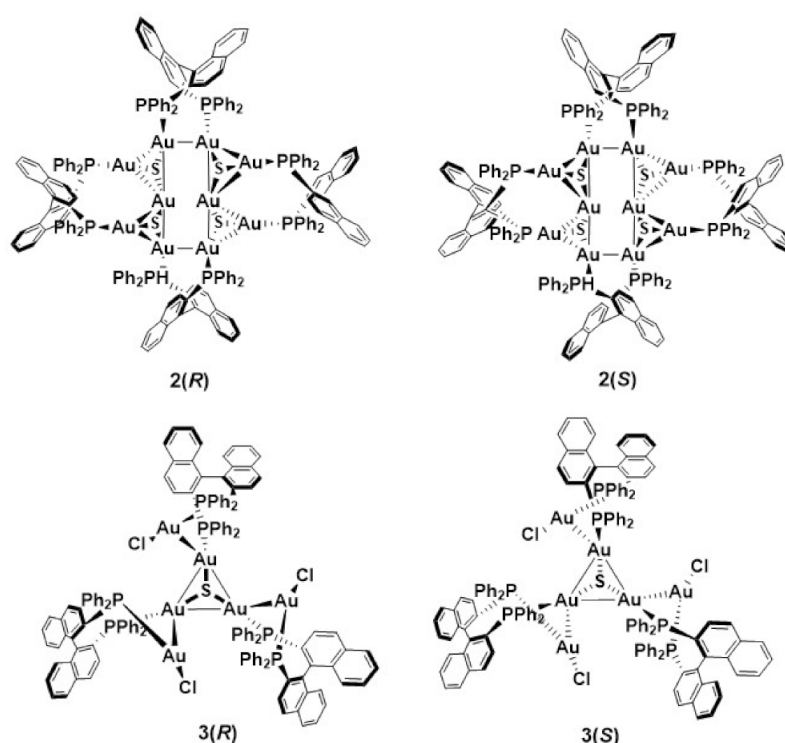


**Figure 2.** Chemical structure of the chiral luminescent clusters reported by Yam et al. in 2016 [18].

Bright luminescent gold(I) phosphinopyridyl clusters **4** and **5** were reported by Wang et al. in 2017 (Figure 3) [19]. Cluster **4** contained a  $\text{Au}_3(\text{PNC})_3$  ( $\text{PNC} = 2\text{-diphenylphosphinopyridyl}$  monoion) moiety and single crystal X-ray analysis showed  $\text{Au}^{\text{I}}\cdots\text{Au}^{\text{I}}$  contacts from 3.033(2) to 3.329(2) Å. The cluster exhibited intense green emission ( $\lambda_{\text{max}} = 497$  nm) in dichloromethane solution, with a measured quantum yield of 21% and triplet emission parentage, as confirmed by analysis of the emission lifetime. Cluster **5** was prepared by treating **4** with  $\text{Ph}_3\text{PAuBF}_4$ . This compound presented unsupported  $\text{Au}^{\text{I}}\cdots\text{Au}^{\text{I}}$  interactions (2.738(2) Å) that linked two  $\text{Ph}_3\text{PAu}^+$  moieties to two gold(I) triangles of **4**, as shown in Figure 3. These unsupported aurophilic contacts made an important contribution to the photophysical properties of **5** and the compound emitted brightly orange in  $\text{CH}_2\text{Cl}_2$  in the presence of an excess of  $\text{Ph}_3\text{PAuBF}_4$  (Figure 4). The emission quantum yield was measured to be 48% in aerated solution and an important increase of the emission lifetime with reference to **4** was also observed. Interestingly, *in vitro* studies with living cells revealed that both cationic clusters selectively stained mitochondria (Figure 4) and, according to the authors, could find application as luminescent probes for these important organelles.

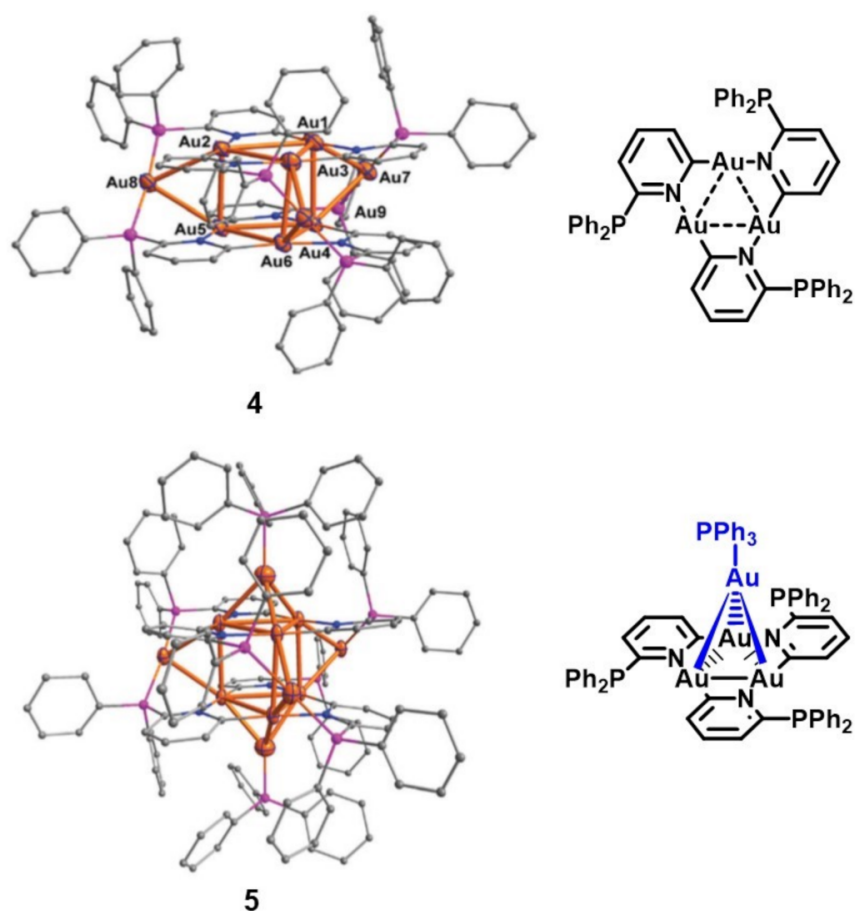


**Figure 3.** Top: X-ray crystal structure of **4** (left) and schematic chemical structure of the cluster's top side (right). Bottom: X-ray crystal structure of **5** (left) and schematic chemical structure showing the unsupported aurophilic interactions in the top and bottom sides of the cluster (right). Adapted from ref. [19] with permission from the Royal Society of Chemistry.

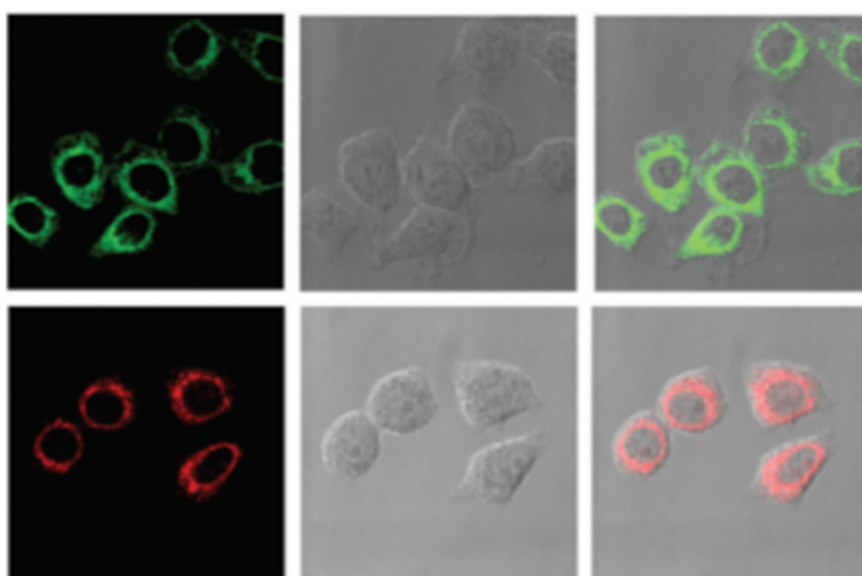


**Figure 4.** (top): Confocal luminescence images of HeLa cells incubated with cluster **4**. (bottom): Confocal luminescence images of HeLa cells incubated with cluster **5**. Reproduced from ref. [19] with permission from the Royal Society of Chemistry.

In 2019, new chalcogenido clusters **6** and **7** with formula  $[\text{Au}_6\{\mu\text{-Ph}_2\text{PN}(\text{CH}_2\text{-o-Py})\text{PPh}_2\}_3(\mu_3\text{-E})_2](\text{ClO}_4)_2$  ( $\text{E} = \text{S}, \text{Se}$ ), were reported by Yam et al. (Figure 5) [20]. The presence of intramolecular aurophilic interactions was corroborated by X-ray crystal analyses, with  $\text{Au}^{\text{I}}\cdots\text{Au}^{\text{I}}$  distances in the range 3.09–3.13 Å. The compounds displayed long-lived red emission in degassed  $\text{CH}_2\text{Cl}_2$  solution with  $\lambda_{\text{max}} = 824$  nm for **6** and  $\lambda_{\text{max}} = 743$  nm for **7**, under excitation at  $\lambda < 400$  nm. The emission of the clusters was increased and blue-shifted ( $\lambda_{\text{max}} = 622$  nm for **6** and  $\lambda_{\text{max}} = 575$  nm for **7**) in EtOH-MeOH- $\text{CH}_2\text{Cl}_2$  glass at 77 K. In both cases, the emission was assigned to be originated from triplet states of ligand to metal charge transfer (LMCT) character mixed with metal-centered (ds/dp) states modified by  $\text{Au}(\text{I})\cdots\text{Au}(\text{I})$  interactions, i.e. LMMCT states. According to the authors, the significant large Stokes shifts shown by the complexes could arise from highly distorted excited state structures, which would be favored in solution. Moreover, the larger emission red shift detected in the selenido derivative would be consistent with the more sigma-donating character if this ligand was in front of the sulfido ligand and the assignment of the LMMCT emission origin.

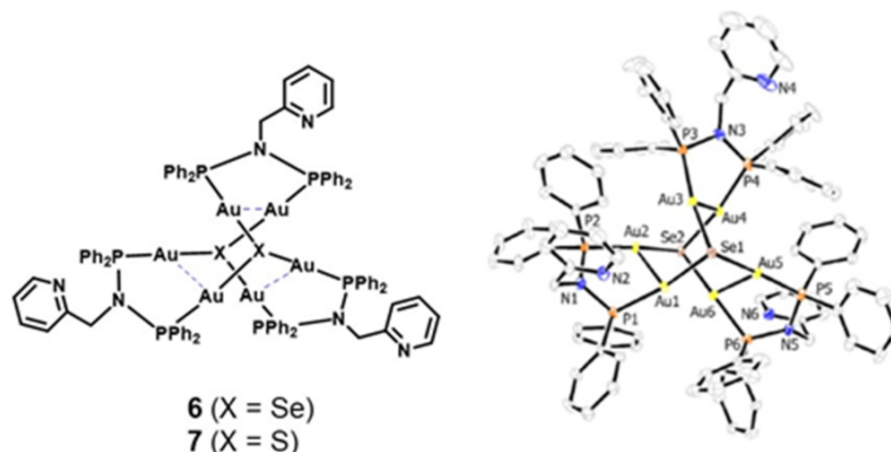


**Figure 5.** Chemical structure of clusters **6** and **7** (left) and X-ray crystal structure of **6** (right). Adapted with permission from ref. [20]. Copyright 2019 John Wiley and Sons.

Tetradecanuclear (**8**) and octadecanuclear (**9**) gold(I) sulfido clusters (Figure 6) were reported by Lang, Ren et al. in 2019 [21]. Single-crystal X-ray diffraction experiments revealed the presence of intramolecular aurophilic bonding in both clusters, with  $\text{Au}^{\text{I}}\cdots\text{Au}^{\text{I}}$  contacts in the range 2.937(8)–3.361(8) Å and 2.985(7) to 3.367(7) for **8** and **9**, respectively. The complexes were emissive in DMSO/PBS buffer (1/99 *v/v*; pH 7) solutions with emission maxima at 536 nm (**8**) and 516 nm (**9**) and DFT calculations suggested a metal to ligand charge transfer (MLCT) origin for the emission. Interestingly, the complexes showed good properties as lysosome trackers in living cells (Figure 6).

Compound **10** and **11** (Figure 7A) were reported by Mitzel, Kottke and co-workers in 2019 [22]. The authors observed an interesting rearrangement from 1,8-diethynylanthracene-Au(I)-phosphane derivatives to the final complexes, comprised by a macrocyclic di-gold(I) anion linked to two gold(I) units via aurophilic interactions. In the case of **10**, elimination of one phosphane unit and coordination of the exocyclic gold(I) ions to the anionic part of the alkynyl spacers of the macrocycle was also observed. The structure of the final complexes was determined by X-ray diffraction analysis, showing  $\text{Au}^{\text{I}}\cdots\text{Au}^{\text{I}}$  distances of 2.861(1) Å and 3.046(1) Å for **10** and **11**, respectively. Interestingly, the rearrangement and formation of **11** could be followed by time-resolved <sup>31</sup>P NMR spectroscopy and by monitoring the changes in the UV-vis absorption and emission spectra in  $\text{CH}_2\text{Cl}_2$  over time. In the last case, a considerable increase of the emission ( $\lambda_{\text{exc}} = 376$  nm) with appearance of a well-structured band ( $\lambda_{\text{max}} = 433, 455, 483$  nm) was observed upon formation of **11** (Figure 7B).

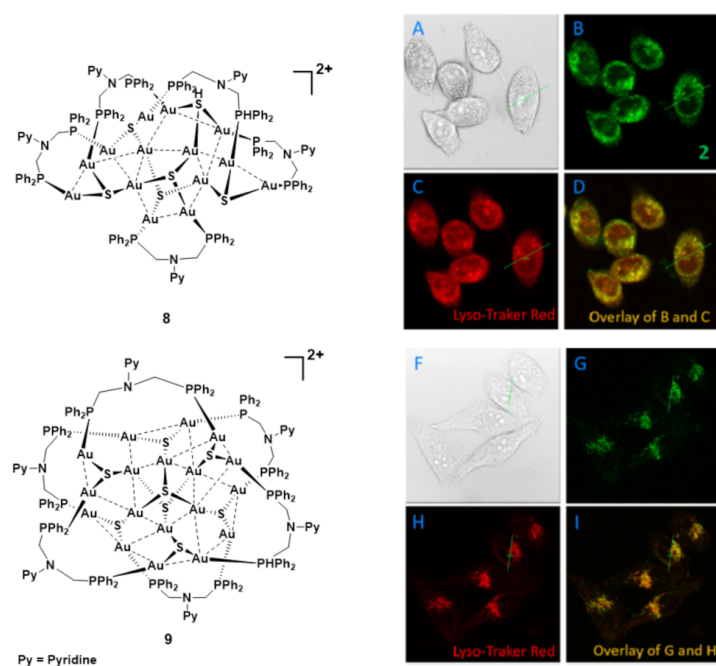


**Figure 6.** Left: Chemical structure of clusters 8 and 9. Right: Colocalization confocal luminescence images of HeLa cells incubated with 8 (top) and 9 (bottom): (A,F) bright-field transmission images; (B,G) confocal images (green channel) of cells with 8 or 9; (C,H) confocal images (red channel) of cells with Lyso-Tracker Red; (D,I) merged images of red and green channels. Adapted with permission from ref. [21]. Copyright 2019 American Chemical Society.

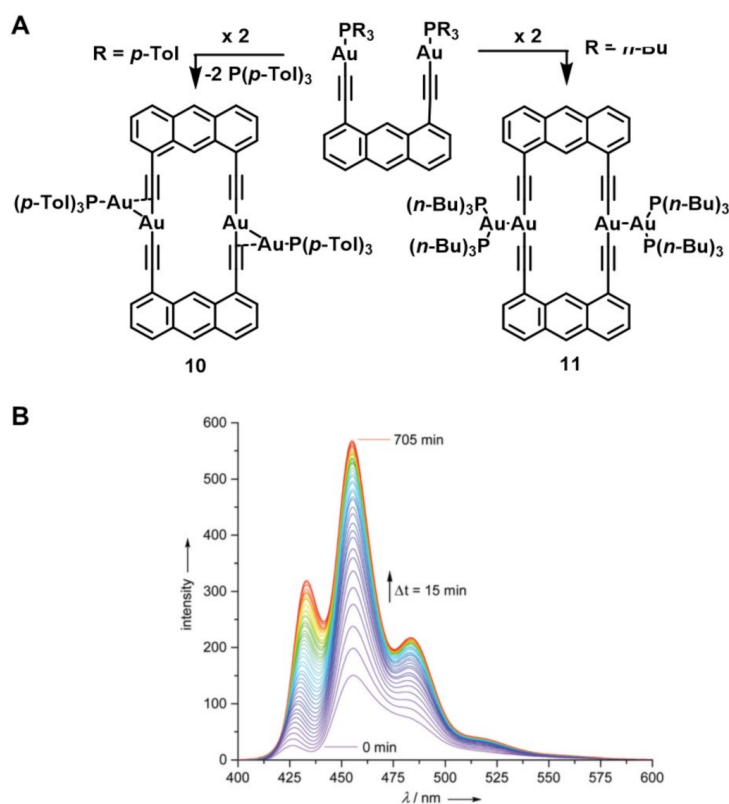
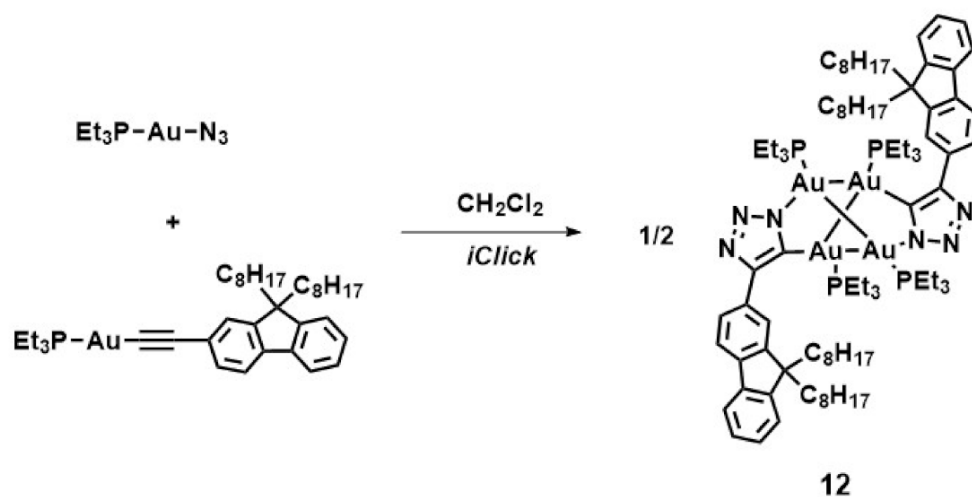


**Figure 7.** (A) Formation of 10 and 11 from the diethynylantracene-Au(I)-phosphane precursors; (B) Increase of the emission in CH<sub>2</sub>Cl<sub>2</sub> solution upon formation of 11 (λ<sub>exc</sub> = 376 nm). Adapted from ref. [22] with permission from the Royal Society of Chemistry.

Veige and co-workers reported the tetranuclear gold(I) cluster **12** in 2020 (Scheme 1) [23]. The compound was prepared using the inorganic Click (iClick) reaction between the corresponding fluorenyl-gold-acetylide precursor and  $\text{PEt}_3\text{AuN}_3$ . The cluster exhibited in THF solution both moderate fluorescence ( $\lambda_{\text{max}} = 408 \text{ nm}$ ,  $\phi_{\text{fl}} = 0.16$ ) and low phosphorescence ( $\lambda_{\text{max}} = 495$  and  $533 \text{ nm}$ ,  $\phi_{\text{ph}} = 0.046$ ) that resulted in an overall white emission. Interestingly, it was found that the compound was also able to generate singlet oxygen ( $\phi_{\Delta} = 0.28$ ). A deep photophysical analysis together with computational studies supported the hypothesis that the fluorescence was originated in a LMCT state and strongly influenced by the presence of aurophilic bonding in the structure. The phosphorescence was tentatively assigned to a  $^3\pi-\pi^*$  state localized on the triazololate-fluorene moiety. The complex was employed as white light dopant in the fabrication of organic light emitting diodes (OLEDs), although the overall performance exhibited by the devices was marginal, which, according to the authors, could be due either to the low photoluminescence efficiency of the cluster and/or poor carrier balance in the device.



**Scheme 1.** Synthesis of cluster **12** by iClick reaction. Adapted with permission from ref. [23]. Copyright 2020 American Chemical Society.

### 3. Self-assembly of Gold(I) Complexes

#### 3.1. Complexes that Display AIE Properties

Gold(I) complexes are attractive candidates to develop Aggregation Induced Emission luminogens (AIEgens) [7,24,25], due to the formation of aurophilic contacts in solution that modulate the emission exhibited by the aggregates. For gold(I) AIEgens, self-assembly has been classically characterized by following the emission changes in samples containing different proportions of a good solvent (usually organic) and a poor solvent (usually water). These changes have been mainly supported by the variations observed in the UV-vis absorption spectra. On many occasions information about the size of the aggregates have been also reported using dynamic light scattering analysis (DLS) and less frequently, Small Angle X-ray Scattering (SAXS). Sometimes, additional information regarding other functional groups involved in the aggregation process has been provided by means of NMR studies. Thus, these are systems that aggregate, although this aggregation does not give rise to the formation of well-defined superstructures such as fibers or micelles, which will be presented in the next section, but rather originate oligomers or aggregates with undefined shapes.

A large majority of gold(I) AIEgens are based in perhalogenated cyanide gold(I) complexes, where  $\pi-\pi$  and  $\text{C-H}\cdots\text{F}$  interactions make also an important contribution to the observed AIE properties. The examples reported in the last five years can be divided according to the presence of additional functional groups in the structure of the



compounds. An important family of derivatives corresponds to perhalogenated cyanide gold(I) derivatives bearing fluorene units which are presented in Figure 8.

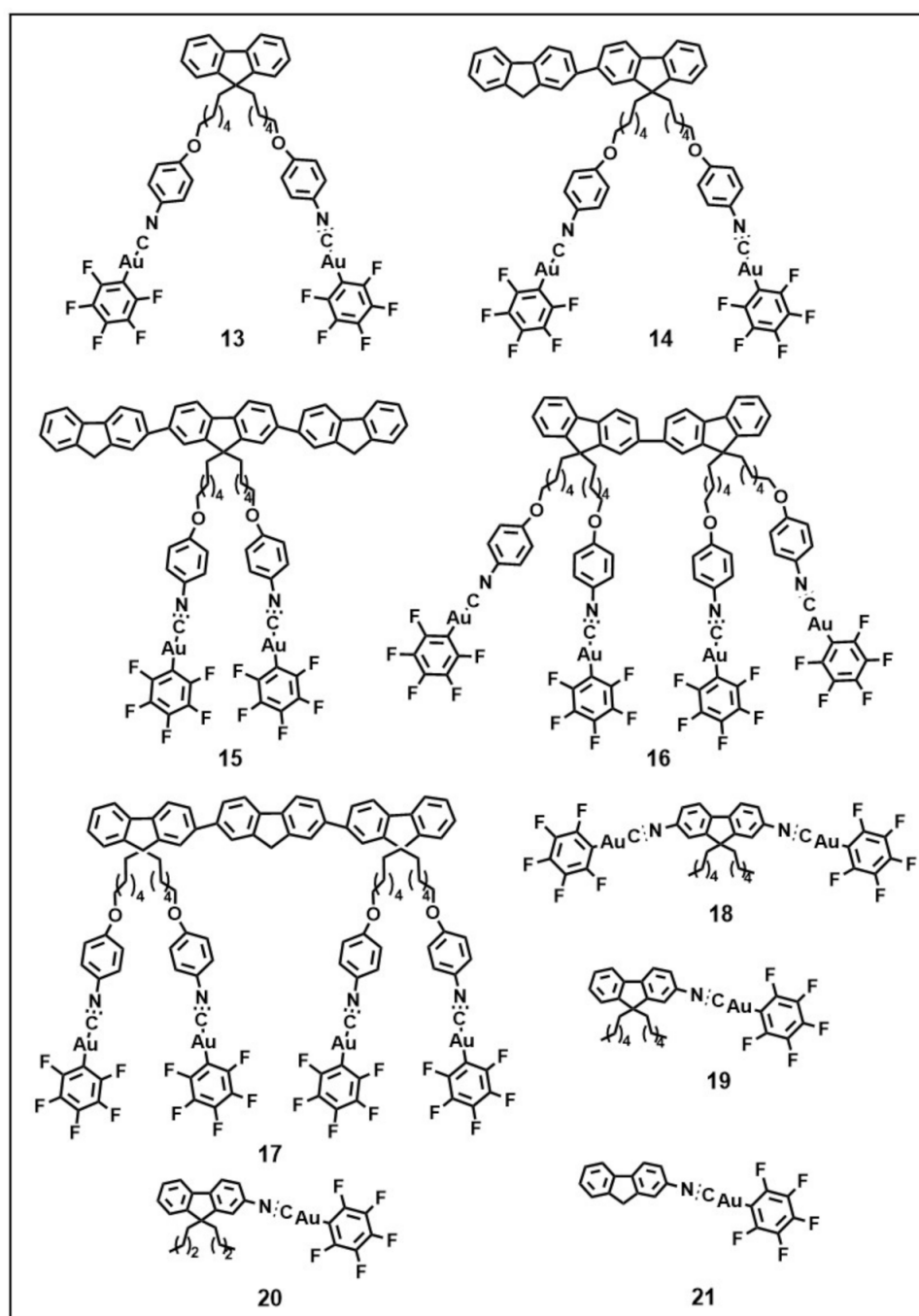


**Figure 8.** Fluorene-based perhalogenated cyanide gold(I) complexes with AIE properties.

In 2015, Liu et al. reported the AIE behavior of the fluorene-based complexes **13–15** and **17** [26], following the work that they published in 2014 with compound **16** [27]. The authors studied the aggregation of the complexes in DMF: H<sub>2</sub>O mixtures and observed that increasing the fraction of water ( $f_w$ ) to 20–30%, originated a new emission due to the formation of aggregates. According to the authors, this emission was related with the presence of aurophilic interactions in the aggregates. In the case of **13–15**, the new emission band was centered at 500–525 nm, whereas in the case of **17**, the combination of the new emission bands with maxima at 399 nm, 418 nm and 538 nm gave rise to an interesting

white light luminogen (Figure 9), similarly to that reported previously for compound **16**. The aggregation phenomenon was also detected in the UV-vis absorption spectra of the compounds due to the increase in the baseline that resulted from the scattering of the light by suspended aggregates. Additionally, in the case of **13** the size of the aggregates was analyzed by DLS for samples containing 90%  $f_w$ , giving an average value of ca. 400 nm.

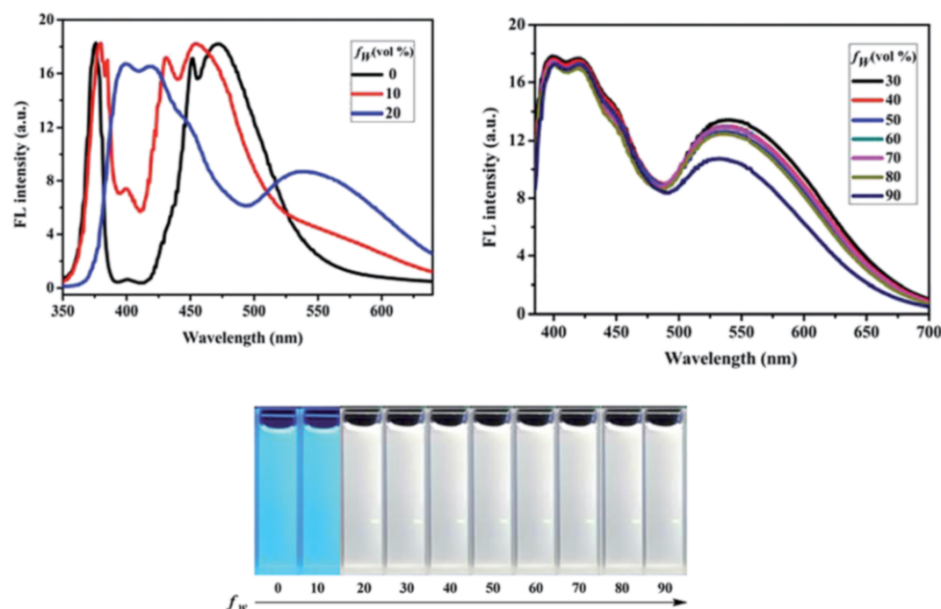


**Figure 9.** Top: Emission spectra ( $\lambda_{\text{exc}} = 330$  nm) of dilute solutions of **17** ( $1.0 \times 10^{-5}$  M) in DMF:H<sub>2</sub>O mixtures with different volume fractions of water: 0%, 10% and 20% (left) and 30–40% (right). Bottom: Picture showing the emission of the same samples when observed under 365 nm UV light. Reproduced from ref. [26] with permission from the Royal Society of Chemistry.

Liu et al. also reported in 2015 about the AIE properties of complex **18** which also showed crystallization-induced emission enhancement [28]. This compound showed in pure DMF one emission band with a maximum at 384 nm, but when water was added to 30% or higher volume fractions, a new emission band with maximum at 570 nm appeared (Figure 10). This band was attributed to aggregates supported by aurophilic interactions. The emission changes were also accompanied by increases in the baseline of the corresponding UV-vis absorption spectra and the size of the aggregates for samples containing 50%  $f_w$  was determined to be around 24 nm by DLS.

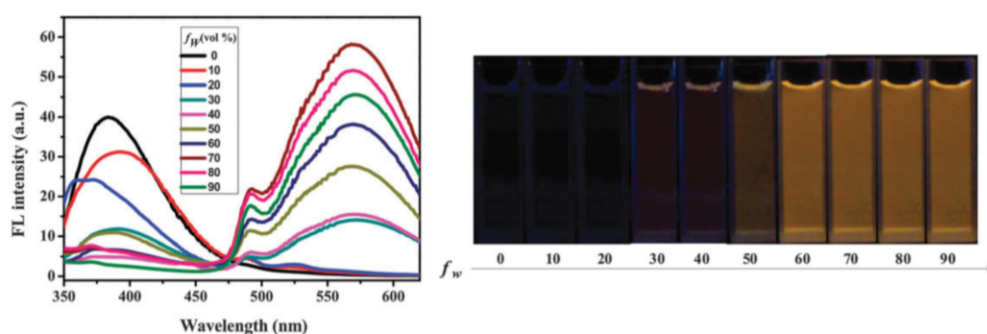


**Figure 10.** Left: Emission spectra ( $\lambda_{\text{exc}} = 330$  nm) of compound **18** ( $c = 2.0 \times 10^{-5}$  M) in DMF:H<sub>2</sub>O mixtures with different volume fractions of water. Right: Picture showing the emission of the same samples when exposed to 365 nm UV light. Adapted from ref. [28] with permission from the Royal Society of Chemistry.

A similar AIE behavior was observed for complexes **19–21** [29], with disappearance of the original emission band with maximum at 350–375 nm in pure DMF and appearance of a broader emission band centered at 500–550 nm upon increasing the volume fractions of water. In this case, a size comprised between 3 nm and 10 nm was measured by DLS for samples of the complexes containing 90%  $f_w$  (Figure 11).

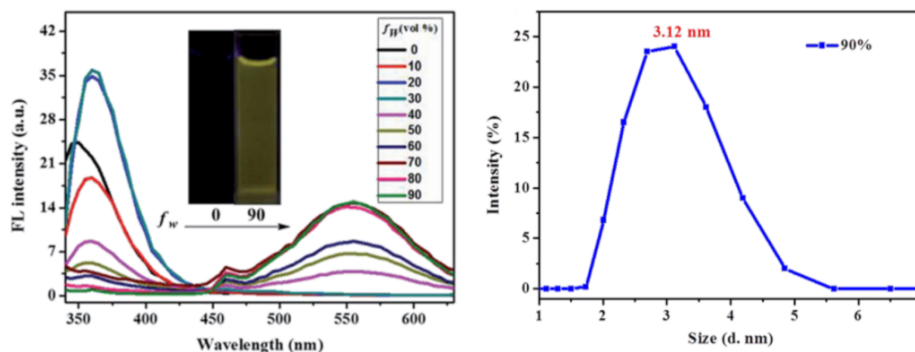


**Figure 11.** (Left): Emission spectra ( $\lambda_{exc} = 330$  nm) of compound **17** ( $c = 2.0 \times 10^{-5}$  M) in DMF:H<sub>2</sub>O mixtures with different volume fractions of water. The inset shows the picture corresponding to the samples with 0% and 90%  $f_w$  observed under 365 nm UV light. (Right): DLS size distribution curve of compound **17** ( $c = 2.0 \times 10^{-5}$  M) in DMF:H<sub>2</sub>O with 90%  $f_w$ . Adapted from ref. [29] with permission from the Royal Society of Chemistry.

A second group of perhalogenated cyanide gold(I) complexes with interesting AIE properties corresponds to those bearing carbazole moieties (Figure 12).

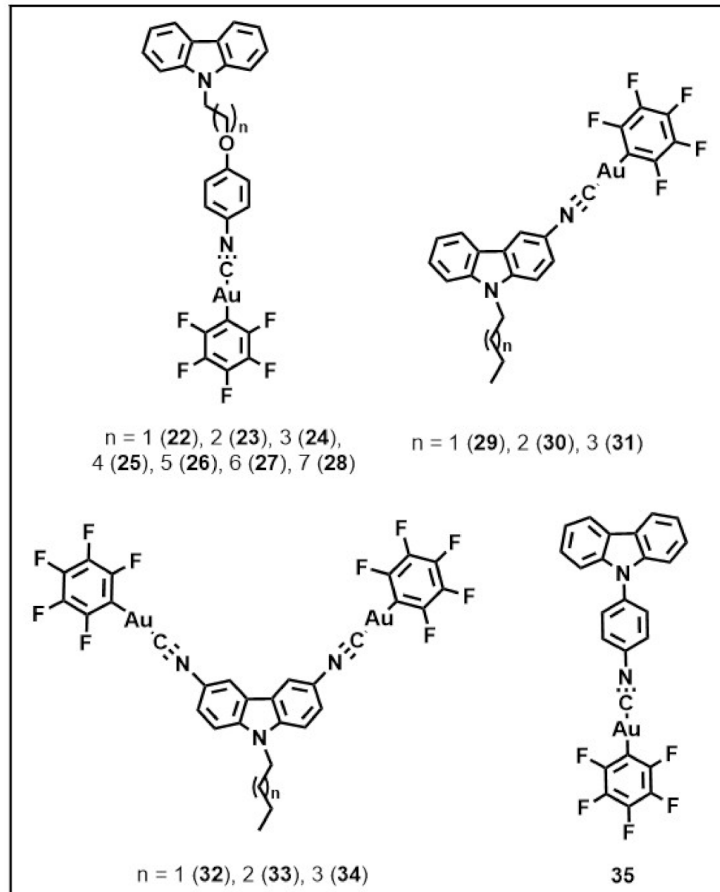


**Figure 12.** Carbazole-based perhalogenated cyanide gold(I) complexes with AIE properties.

Carbazole-based derivatives **22–28** were reported by Liu et al. in 2015 [30]. The compounds were practically non-emissive in DMF solutions. However, when the water volume fraction was increased to 40–70%, a new green emission with a maximum at ca. 515 nm appeared. This emission was related with the formation of nanoaggregates presenting gold-gold intermolecular interactions and was accompanied by an increase of the baseline in the corresponding UV-vis absorption spectra (Figure 13). The size of the nanoaggregates was measured by means of DLS analysis for samples of the complexes containing a high content of water (90%), giving values in the range of 28–51 nm.

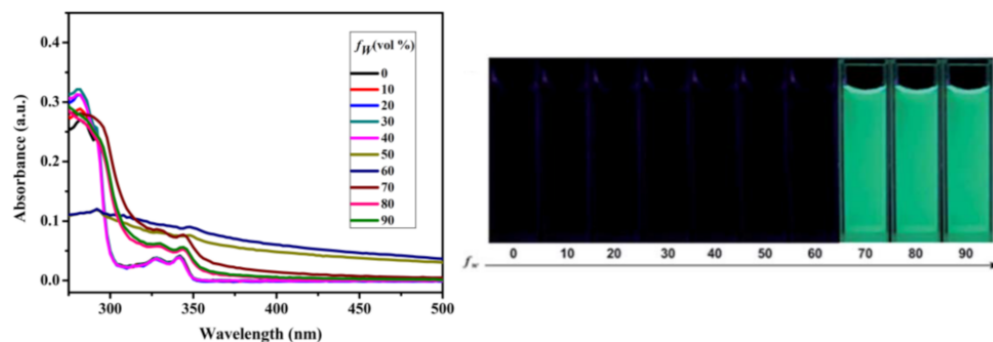


**Figure 13.** (left): UV-vis absorption spectra of compound **22** ( $c = 1.0 \times 10^{-5}$  M) in DMF:H<sub>2</sub>O mixtures with different volume fractions of water. (right): Picture showing the emission of the same samples when exposed to 365 nm UV light. Adapted from ref. [30] with permission from the Royal Society of Chemistry.

The AIE properties of the carbazole-based mononuclear (**29–31**) and dinuclear (**32–34**) gold(I) complexes were reported by Liu et al. in 2016 [31]. For the mononuclear compounds **29–31** and the dinuclear compound **32**, a new emission band centered at ca. 530 nm appeared upon addition of water to DMF solutions of the complexes. It seemed that less water content was needed in the case of the dinuclear complex for aggregation of the sample and consequent emergence of the green emission (60–70% in the case of **29–31** in front of 20% for **32**).

Interestingly, for the dinuclear gold(I) complexes with longer alkyl chains **33** and **34**, an emission centered around 485 nm appeared when low water content was used (20%  $f_w$ ) which was gradually red-shifted up to 530 nm when higher volume fractions of water were employed. These changes were also accompanied by variations in the position of the UV-vis absorption maximum and broadening of the less energetic absorption band as well as an increase in the baseline of the spectra, which was much more pronounced in the case of the samples containing 20%  $f_w$ . Although the authors do not give any explanation for the behavior, it seems that different type of aggregates could be formed in the presence of low and high water contents [32]. For **33** and **34**, DLS measurements revealed aggregates of different sizes for samples containing 20%  $f_w$  (14–16 nm) and 90%  $f_w$  (4–7 nm), respectively (Figure 14).

AIE properties of complex **35** were reported by Liu, Pu et al. in 2017 [33]. In pure DMF solution, the compound emitted at 395 nm, but when water volume fraction was increased to 50%, a blue emission with maximum at ca. 425 nm appeared. According to the authors, this new emission was probably due to the restriction of the carbazole unit rotation. At higher water contents the emission at 425 nm gradually disappeared and a new band centered at 530 nm appeared which was attributed to the presence of aurophilic interactions (Figure 15). In the UV-vis absorption spectra a red-shift and broadening of the less energetic transition was detected. The authors also observed that the size of the nano-aggregates measured by DLS decreased when the water content was increased (8 nm for 60%  $f_w$  in front of 3 nm for 90%  $f_w$ ).

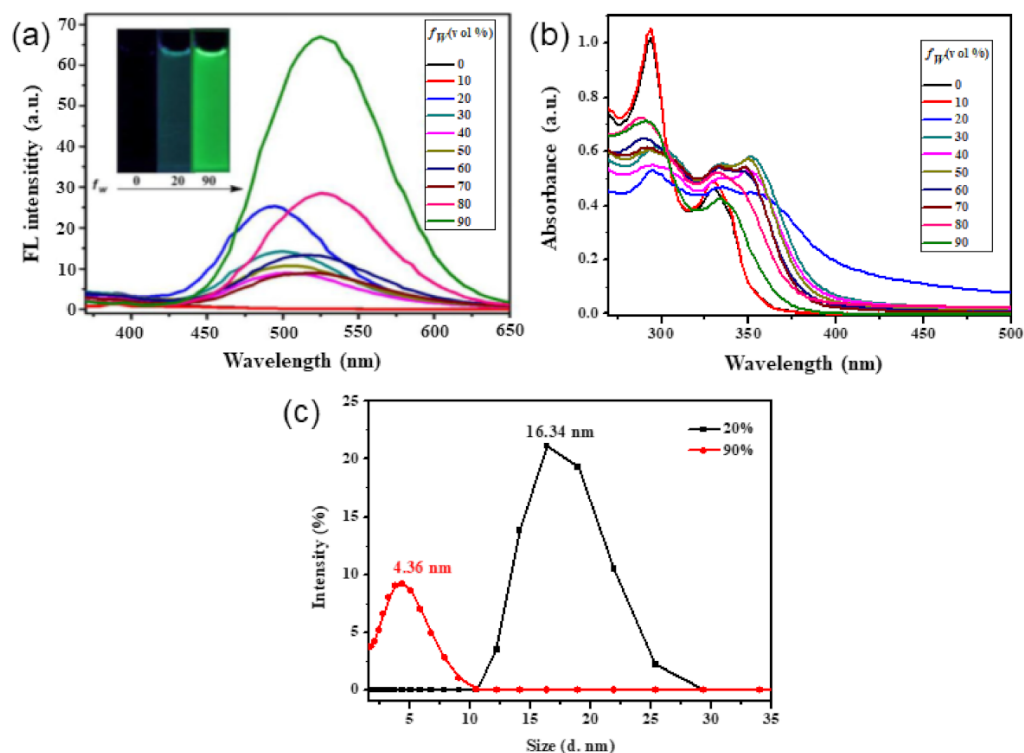


**Figure 14.** (a): Emission spectra ( $\lambda_{\text{exc}} = 350 \text{ nm}$ ) of complex **34** ( $c = 2.0 \times 10^{-5} \text{ M}$ ) in DMF:H<sub>2</sub>O mixtures with different volume fractions of water. The inset shows the picture corresponding to the samples with 0% 20% and 90%  $f_w$  observed under 365 nm UV light; (b): UV-vis absorption spectra corresponding to the same solutions; (c): Size distribution curves of the complex **34** ( $c = 2.0 \times 10^{-5} \text{ M}$ ) in DMF:H<sub>2</sub>O with 20%  $f_w$  and 90%  $f_w$ . Adapted with permission from ref. [31]. Copyright 2016 Elsevier B.V.

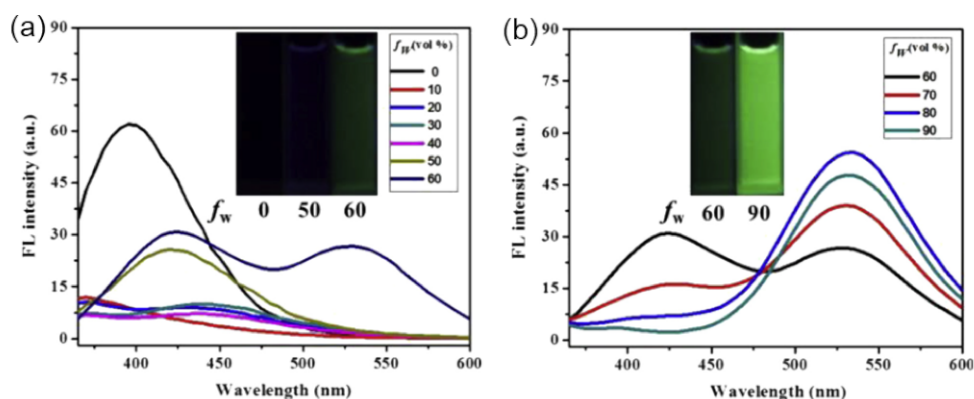


**Figure 15.** (a): Emission spectra ( $\lambda_{\text{exc}} = 330 \text{ nm}$ ) of complex **35** ( $c = 1.0 \times 10^{-5} \text{ M}$ ) in DMF:H<sub>2</sub>O mixtures with different volume fractions of water (0–60%). The inset shows the picture corresponding to the samples with 0% 50% and 60%  $f_w$  observed under 365 nm UV light; (b): Emission spectra ( $\lambda_{\text{exc}} = 330 \text{ nm}$ ) of complex **35** ( $c = 1.0 \times 10^{-5} \text{ M}$ ) in DMF:H<sub>2</sub>O mixtures with different volume fractions of water (60–90%). The inset shows the picture corresponding to the samples with 60% and 90%  $f_w$  observed under 365 nm UV light. Reproduced with permission from ref. [33]. Copyright 2016 Elsevier B.V.

Other perhalogenated cyanide gold(I) complexes, containing functionalities different than fluorene and carbazole and possessing AIE properties have been also reported in the last years and are presented in Figure 16.



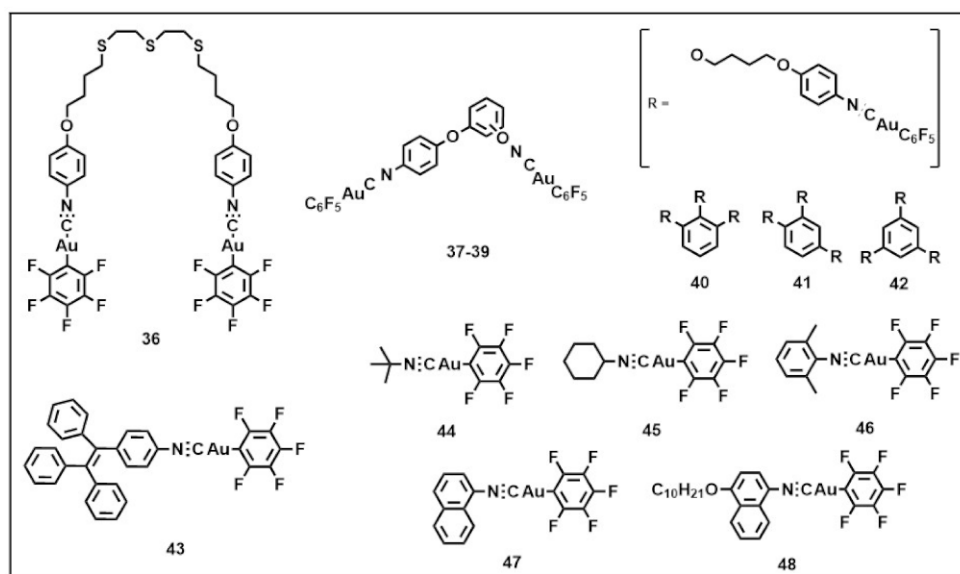


**Figure 16.** Perhalogenated cyanide gold(I) complexes with AIE properties, containing functionalities different than fluorene and carbazole.

The group of Liu et al. reported in 2015 on the AIE behavior of the dinuclear gold(I) complex **36** in acetonitrile:H<sub>2</sub>O mixtures [34]. The compound was not emissive in pure acetonitrile, but the addition of water to 40% *f<sub>w</sub>* produced the appearance of an emission band with  $\lambda_{\text{max}}$  at ca. 570 nm. Increasing the amount of water gave rise to an increase in the emission, which was accompanied by a broadening of the band and blue shift in the emission maximum for the highest volume fractions of water (Figure 17), which could be compatible with the presence of different types of aggregates in samples containing different contents of water. Changes were also observed in the UV-vis absorption spectra upon increasing the water content. The absorption of the compound at 270 nm in pure acetonitrile decreased and shifted to the red by increasing the water volume fraction. The size of the aggregates was measured for samples containing CH<sub>3</sub>CN:H<sub>2</sub>O 50:50 giving an average value of ca. 955 nm.

Liu et al. also published in 2015 the results obtained with derivatives **37–39** [35]. The dinuclear complexes were practically non-emissive in a good solvent such as DMSO. However, upon addition of 30–40% volume fraction of water, the compounds became emissive with a broad band centered at 500–510 nm (Figure 18). Changes were also observed in the corresponding UV-vis absorption spectra with a red shift of the absorption band of the compounds together with an increase in the baseline when the water content was increased. According to the authors, the observed variations are in agreement with the formation of nano-aggregates and changes in the intermolecular gold-gold interactions upon addition of water.

Liu et al. also reported the AIE behavior of trinuclear gold(I) compounds with similar structure (**40–42**) in 2015 [36]. The AIE properties of these complexes were analyzed in DMF:H<sub>2</sub>O mixtures. Upon addition of water, a new green emission centered at ca. 500 nm was detected. In addition, changes in the position of the absorption maximum were observed by means of UV-vis spectroscopy, together of an increase of the baseline of the corresponding spectra. The size of the aggregates was determined to be in the range 70–170 nm for samples containing 50% *f<sub>w</sub>*. According to the authors, the aggregation of the compounds originated changes in the intermolecular gold-gold distances with the consequent appearance of the green emission.

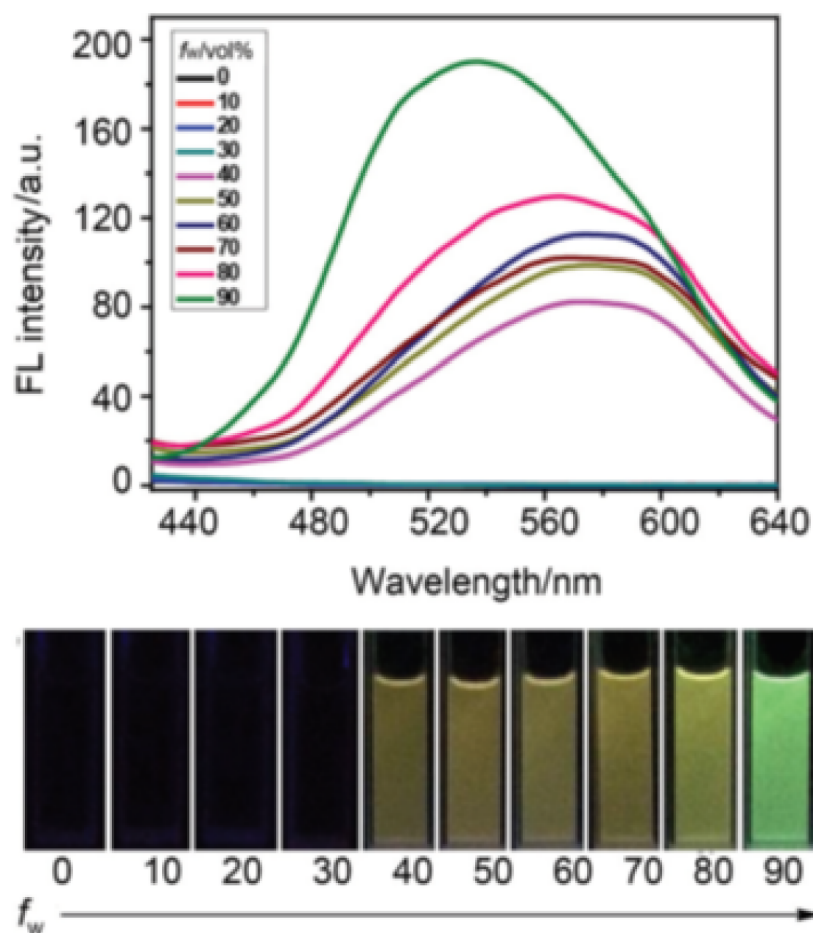


**Figure 17.** (up): Emission spectra ( $\lambda_{\text{exc}} = 340 \text{ nm}$ ) of compound **36** ( $c = 2.0 \times 10^{-5} \text{ M}$ ) in  $\text{CH}_3\text{CN}:\text{H}_2\text{O}$  mixtures with different volume fractions of water. (bottom): Picture showing the emission of the same samples when exposed to UV light. Reproduced with permission from ref. [34]. Copyright 2015 John Wiley and Sons.

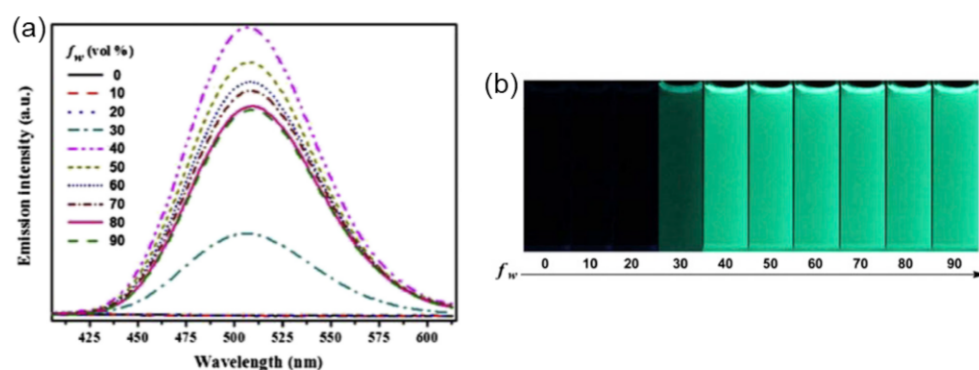


**Figure 18.** (a): Emission spectra ( $\lambda_{\text{exc}} = 315 \text{ nm}$ ) of compound **39** ( $c = 1.0 \times 10^{-5} \text{ M}$ ) in  $\text{DMSO}:\text{H}_2\text{O}$  mixtures with different volume fractions of water; (b): Picture showing the emission of the same samples when exposed to 365 nm UV light. Adapted with permission from ref. [35]. Copyright 2015 Elsevier B.V.

The AIE properties of the tetraphenylethene-based gold(I) derivative **43** were reported by Zhang, Yuan et al. in 2017 [37]. As tetraphenylethene is a typical AIE luminogen, it was envisaged by the authors that **43** could also be AIE active. In fact, the compound exhibited Aggregation Induced Phosphorescence, which was attributed to the spin-orbit

coupling promoted by the heavy gold atom and subsequent intersystem-crossing process. The emissive properties of the complex were studied in THF:H<sub>2</sub>O mixtures. The emission of the complex was very weak in pure THF and it was necessary to increase the volume fraction of water above 70% to measure a remarkable green emission with maximum at 492 nm (Figure 19). DLS experiments showed the presence of nano-aggregates in samples containing 70, 80 and 90% of water. Moreover, the size of the aggregates decreased when the fraction of water was increased (457 nm for 70%  $f_w$  vs 107 nm for 90%  $f_w$ ), in agreement with that reported for other Au(I) complexes [31,33].

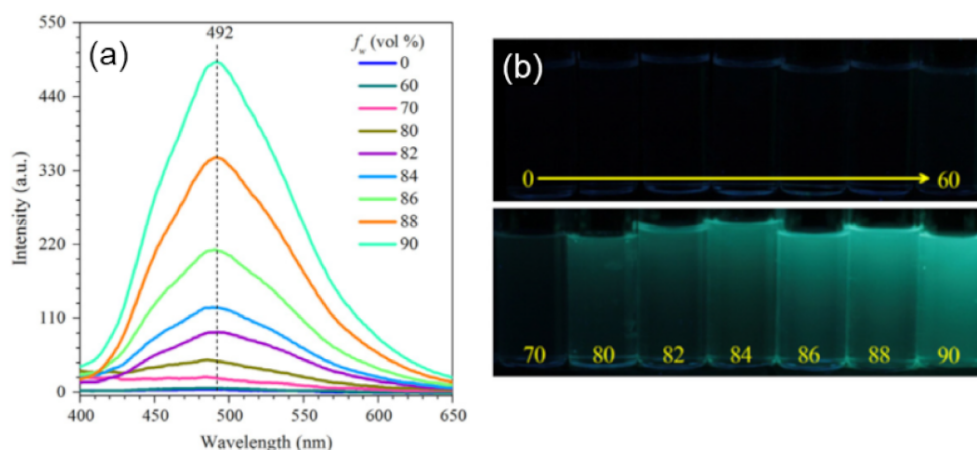


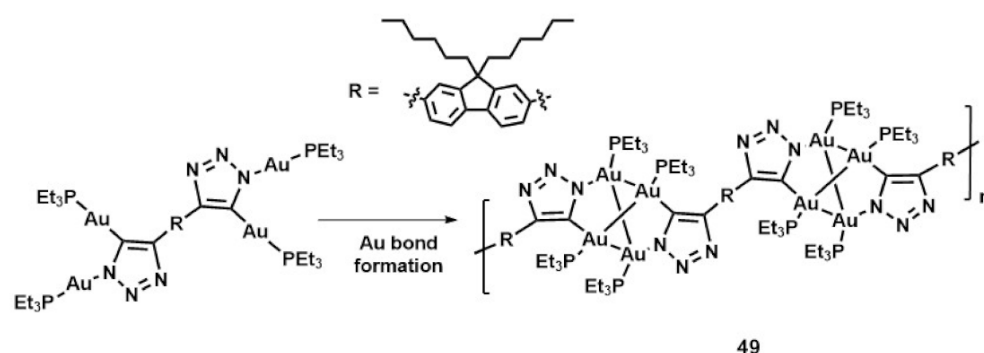
**Figure 19.** (a): Emission spectra ( $\lambda_{exc} = 350$  nm) of compound **43** ( $c = 2.0 \times 10^{-5}$  M) in THF:H<sub>2</sub>O mixtures with different volume fractions of water; (b): Picture showing the emission of the samples when exposed to 365 nm UV light. Adapted with permission from ref. [37]. Copyright 2017 Elsevier B.V.

Complexes **44–48** with a -NC-Au-C<sub>6</sub>F<sub>5</sub> unit and bearing different alkyl or aryl moieties were reported by Liu, Yin et al. in 2018 [38]. The AIE properties of the complexes were studied in THF:H<sub>2</sub>O mixtures. The formation of aggregates was confirmed by DLS. The alkyl-substituted compounds **44** and **45** exhibited a similar AIE behavior showing a yellow emission centered at ca. 550 nm for a 90% water content.

In the case of the aromatic derivatives **46–48**, the aggregates started to emit in samples containing water volume fractions of 60–70%, although the emission was quenched for the highest water volume fractions (80–90%). Moreover, the emission maximum, placed in the range between 420 nm and 630 nm, was markedly different depending on the aryl substituent. The authors tentatively presumed that the quenching of the luminescence could be related to the tightening of the intermolecular  $\pi$ - $\pi$  aromatic interactions for the highest water contents. In fact, according to the authors the red-shifted UV-vis absorptions recorded for **46–48** in aggregated samples could support this interpretation.

Other gold(I) complexes with variable structure that show emission upon aggregation in solution have been reported in recent years. In 2015, Veige et al. [39] reported the oligomeric complex **49** that was obtained via aurophilic induced self-assembly of the corresponding tetranuclear gold(I) triazolote precursor, giving rise to Au<sub>4</sub> repeating units that were stable in solution (Scheme 2). The oligomeric nature of **49** was demonstrated by <sup>1</sup>H DOSY NMR experiments which provided a hydrodynamic radius of 89.9 Å for the complex. Moreover, temperature variable experiments revealed that the oligomer was stable upon heating up to 50 °C, pointing out the strength of the aurophilic bonds. Emission measurements in CH<sub>2</sub>Cl<sub>2</sub> also indicated that the Au<sub>4</sub> units of the oligomer were preserved in solution by comparing the emission of the sample ( $\lambda_{exc} = 285$  nm) with that shown by a model cluster with Au<sub>4</sub> linkage. In both cases, an emission attributed to Au...Au bond with maximum at 324 nm appeared. The oligomer **49** also presented the typical emission of the fluorene substituent ( $\lambda_{exc} = 353$  nm) which was red shifted (18 nm) upon increase of the concentration (from 5  $\mu$ M to 50  $\mu$ M), the latter being indicative of a higher degree of

oligomerization and consistent with the results obtained in variable concentration DOSY NMR experiments.



**Scheme 2.** Formation of oligomer **49** via aurophilic induced self-assembly of the triazolate gold(I) precursor [39].

In 2017, Jiang, Sun and co-workers [40] reported clusters with general formula  $(\text{Au})_n(\text{SC}_{12}\text{H}_{25})_m$  (**50**). In particular, they prepared the luminescent complex  $[(\text{Au})_{15}(\text{SC}_{12}\text{H}_{25})_{14-16}]^+$  by reducing  $\text{HAuCl}_4$  with dodecanethiol in toluene and the non-luminescent  $[(\text{Au})_7(\text{SC}_{12}\text{H}_{25})_6]^+$  species by carrying out the same reaction in EtOH. The authors studied the emission changes exhibited by the system in EtOH:toluene mixtures and observed an enhancement in the emission at ca. 620 nm when the fraction of toluene was increased. This behavior was attributed by the authors to aggregation of bilayer supramolecular structures of Au(I)– $\text{SC}_{12}\text{H}_{25}$  units which would favor the intra- and intermolecular aurophilic interactions with the consequent enhancement of the luminescence.

Yam and coworkers explored in 2017 the AIE properties of the alkynylgold(I) derivative **51** (Figure 20A) [41]. The aggregation of the complex was studied in water/methanol mixtures, following the changes in the UV-vis absorption as well as in the emission spectra upon increasing the water fraction. For the latter, a significant increase of the emission at 640 nm was observed. This luminescence enhancement was attributed to the establishment of aurophilic interactions by self-assembly of the complex, which gave rise to the appearance of a ligand-to-metal–metal charge transfer (LMMCT) emission (Figure 20B).

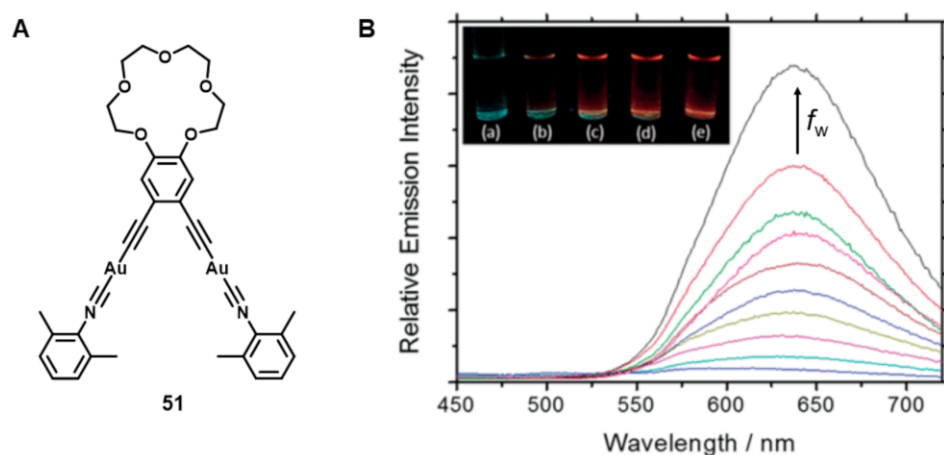


**Figure 20.** (A) Chemical structure of **51**; (B) Emission spectra ( $\lambda_{\text{exc}} = 340$  nm) of complex **51** ( $c = 1.01 \times 10^{-5}$  M) in different water/methanol ( $v/v$ ) ratios. Inset: Pictures corresponding to samples with 0%, 30%, 50%, 70% and 90%  $f_w$  observed under UV light. Adapted with permission from ref [41]. Copyright 2017 John Wiley and Sons.

Aggregation induced emission of the chiral Au(I) clusters **52** and **53** (Figure 21A) was reported by Zang, Wang and co-workers in 2020 [42]. The complexes showed intense

green emission centered at 507 nm (Figure 21B) upon addition of water (40%,  $f_w$ ) to DMF solutions ( $2 \times 10^{-5}$  M). The quantum yield of emission and lifetime were determined to be 36.7% and 3.62  $\mu$ s, respectively. The quantum yield continued to increase up to a  $f_w = 60\%$ , reaching a value of 41.4%. For this water fraction, aggregates with size around 200 nm were detected by DLS and TEM analyses. The emergence of the emission was attributed to weak intercluster interactions among the ligands and interclusteraurophilic interactions (Au $\cdots$ Au bonds in the range 2.956–3.052 Å), that were detected in the X-ray structure of the complexes in the solid state. Higher water contents provoked a decrease in the quantum yield, which was attributed to the formation of large aggregates with poor crystallinity. The enantiomers also exhibited excellent circularly polarized luminescence (CPL) properties and were used to prepare circularly polarized (CP)-OLEDs devices which exhibited CP electroluminescence with maximum external quantum efficiency (EQE) for the electroluminescence of 1.5% (Figure 21C).

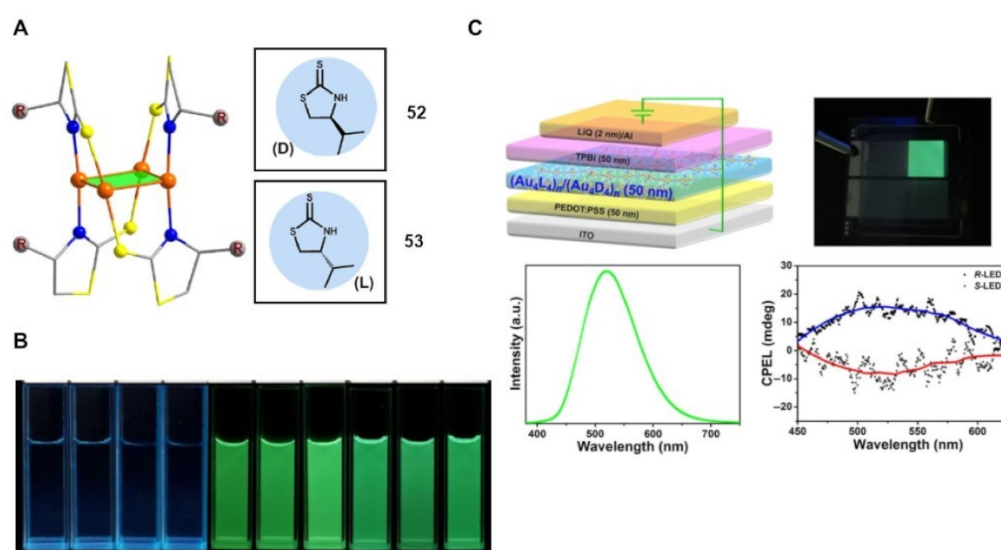


**Figure 21.** (A) Chemical structure tetranuclear gold(I) clusters **52** and **53**; (B) Picture of **53** in DMF ( $c = 2 \times 10^{-5}$  M) with 0–90% of water under UV light; (C) Fabrication and performance of CP-OLEDs based on **52** and **53**. Adapted with permission from ref. [42]. Copyright 2020 Springer Nature.

### 3.2. Gold(I) Complexes that Self-assemble in Well-defined Superstructures

Gold(I) complexes also self-assemble, giving rise to *well-defined* supramolecular structures such as metallogels, vesicles and micelles. These soft materials can find application in a wide variety of fields, including the development of stimuli-responsive soft materials, drug delivery systems, separation processes and cosmetics, among others [13].

Several alkynyl gold(I) phosphane complexes have been reported in the last years to aggregate in water and organic solvents to render large luminescent supramolecular assemblies (Figure 22). Rodríguez's group and co-workers have extensively studied this kind of complexes. Thus, they had reported in 2013 the formation of luminescent hydrogels based on the simple structures **54** and **55**, where a Au(I) atom was bound to a water soluble phosphane (1,3,5-triaza-7-phosphaadamantane (PTA) or 3,7-diacetyl-1,3,7-triaza-5-fosfabiciclo[3.3.1]nonane (DAPTA)) and the chromophore 4-ethynylpyridine. Several studies determined that the formation of auophilic interactions, together with the participation of other weak intermolecular forces, was determinant in the aggregation of the compounds and formation of long luminescent fibers in water [32,43–45]. In 2015, as a continuation of these investigations, Rodríguez, Lima and co-workers, reported the gold(I) complex **56**, which contained the phosphane DAPTA and the chromophore moiety propargyloxycoumarin instead of 4-ethynylpyridine [46]. Upon aggregation in water, the compound was also able to form long luminescent fibers, in a self-assembly process driven by hydrogen bonding,  $\pi$ - $\pi$  stacking and auophilic interactions according to the X-ray



crystal structure analysis which showed Au(I)⋯Au(I) contacts at 3.1274(4) Å and 3.1316(4) Å. DLS and microscopy studies revealed that the compound formed nanometric aggregates at micromolar concentrations that resulted on long micrometric fibers upon increasing the concentration to the millimolar range. Isolated fibers exhibited the blue emission corresponding to the fluorescence of the coumarin, whereas dense reticulated networks of fibers shown green emission assigned to the phosphorescence of the coumarin (Figure 23). This effect was attributed to greater spatial proximity of the gold(I) ions in the dense networks that, due to the heavy atom effect, favored the intersystem crossing with the consequent increasing of the triplet emission.

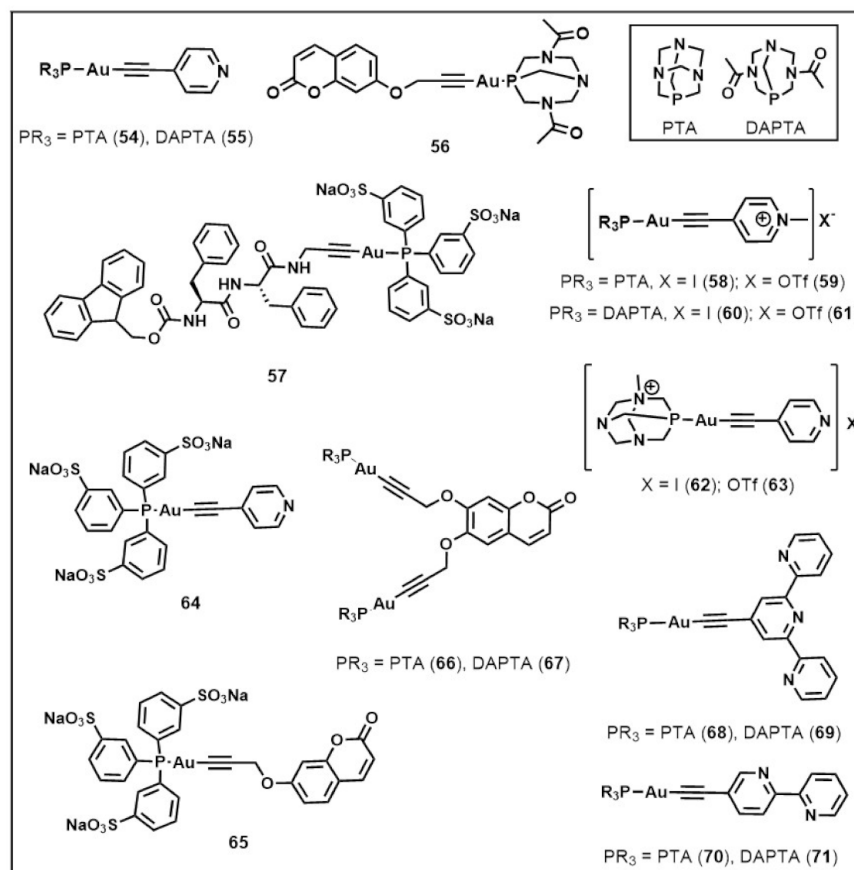


**Figure 22.** Alkyne gold(I) phosphanes that form large luminescent supramolecular assemblies.

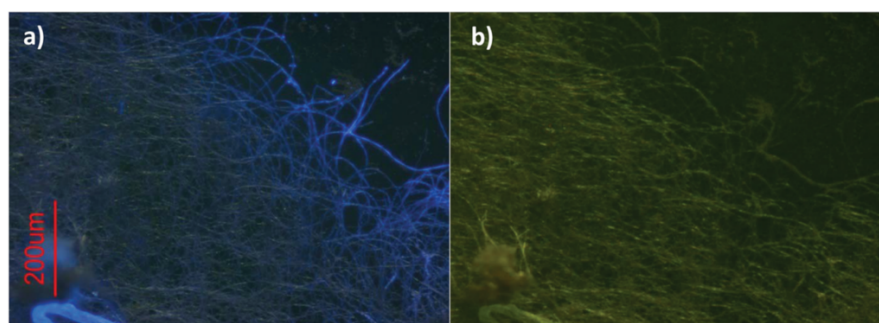


**Figure 23.** Fluorescence micrographs of the fibers formed by 56 observed using a band-pass filter of 300–400 nm (a) and 450–490 nm (b). Reproduced from ref. [46] with permission from the Royal Society of Chemistry.

The same year, Besenius et al. reported the peptidic Au(I) metalloamphiphile 57 [47]. The complex was able to self-assemble in water at physiological conditions giving rise to

micellar structures with an average size of 14 nm, in a process driven by intermolecular forces implying the peptidic moiety as well as the gold(I) units. The self-assembly was favored, increasing the ionic strength from 0.1 M NaCl to 1 M NaCl, which was attributed to a decrease on the repulsive electrostatic forces coming from the anionic charged phosphane as well as an increase of the hydrophobic effect which stabilized the self-assembly. The micelles presented a long-lived broad luminescence (Figure 24), with an emission centered at 520 nm, tentatively assigned to the authors to have an origin on a  $^3[\sigma(\text{Au-P}) \rightarrow \pi^*(\text{C}\equiv\text{C})]$  metal-to-ligand charge-transfer or a  $^3\text{IL} [\pi-\pi^*(\text{C}\equiv\text{C})]$  metal-perturbed intra-ligand states, with a possible contribution of  $\text{Au(I)} \cdots \text{Au(I)}$  interactions.

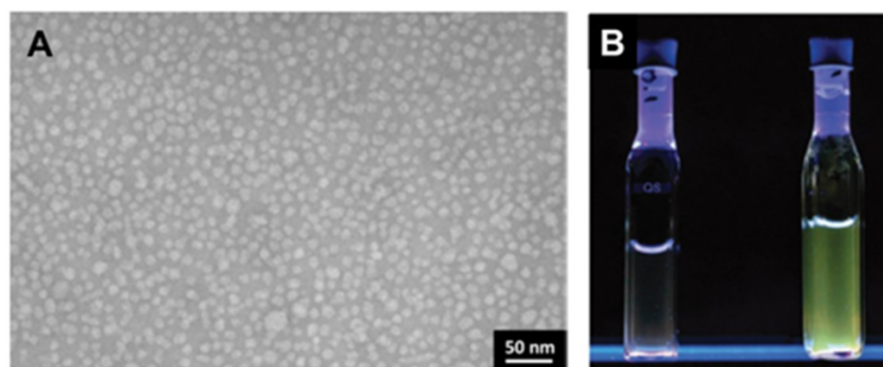


**Figure 24.** (A) TEM micrograph of **57** deposited on carbon coated grids from a 2 mg/mL solution in 10mM Tris buffer, pH 7.5 and 1 M NaCl (negative staining was performed with 2% w/v uranyl acetate); (B) Images of **57** under UV light in 10 mM phosphate buffer (pH 7.4) with 0.1 M NaCl (left) and 1.0 M NaCl (right). Adapted from ref. [47] with permission from the Royal Society of Chemistry.

In 2016, Rodríguez and co-workers reported the complexes **58–63**, with similar structure to **54** and **55**, but cationically charged by methylation of the phosphane or the 4-ethylpyridine ligand [48]. These structural modifications had a dramatic impact on the aggregation properties of the complexes in water (Figure 25). Thus, **58** and **60**, presenting the cationic charge in the pyridine and having iodide as the counterion, self-assembled in the form of vesicle type structures with size around 20 nm. So, it seems that for these compounds, the presence of the positive charge precluded the formation of the long fibers observed for **54** and **55**. The change of the counterion ion to triflate in **59** and **61**, also had a great effect on the structures formed and in this case square-like concentric assemblies with a size of ca. 20–40  $\mu\text{m}$  were detected by SEM analysis. On the other hand, location of the positive charge in the PTA phosphane, with iodide as the counterion (**62**) gave rise to the formation of rod aggregates of 20–30  $\mu\text{m}$  length, whereas the analogous triflate derivative (**63**) was completely soluble in water and did not show aggregation. Emission spectra of diluted samples of the complexes in water ( $\lambda_{\text{exc}} = 376 \text{ nm}$ ) displayed a band centered at ca. 450 nm and assigned to intra-ligand  $^3[\pi-\pi^*(\text{alkynyl})]$  emission origin. For complexes containing the phosphane PTA, namely **58**, **59** and **62** (less soluble in water and therefore aggregated at spectroscopic concentrations), an additional lower energy band centered at ca. 550–600 nm was detected and assigned to MMLCT transitions within the aggregates. Moreover, the complexes also exhibited aggregation in organic solvents, giving rise to different topologies, depending on the solvent. Emission studies also evidenced the presence of the lower energy band at 550–600 nm, whose intensity was higher in more polar solvents, indicating a higher degree of aggregation in these solvents.

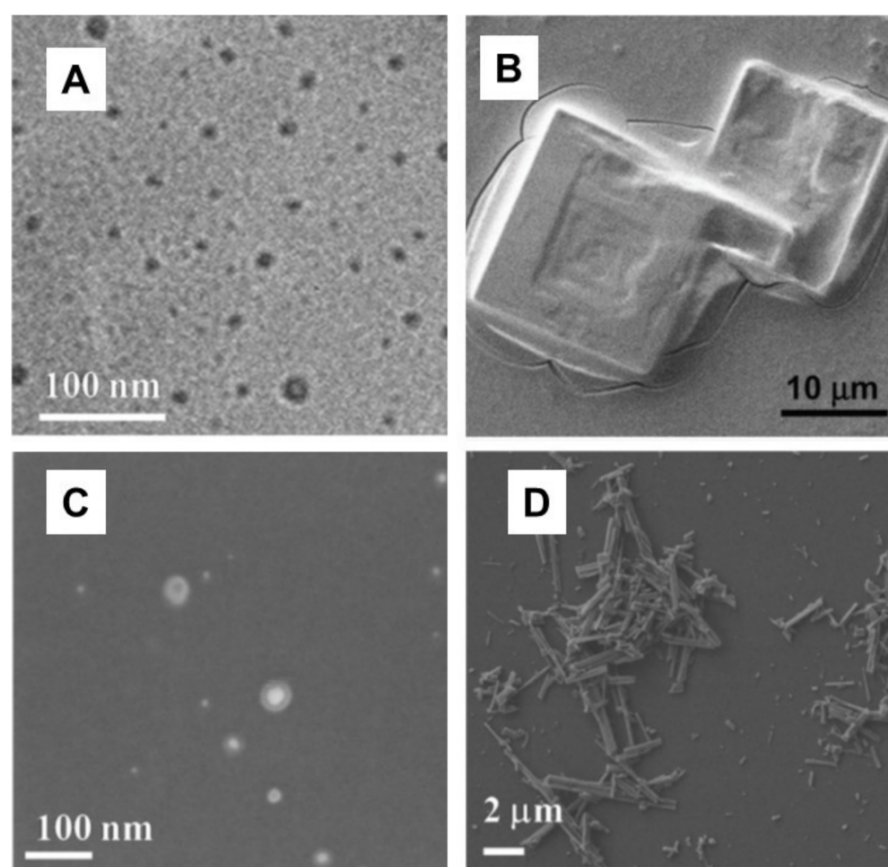


**Figure 25.** Cryogenic TEM image of sample of a  $5 \times 10^{-4}$  M aqueous solution of **58** (A) and SEM micrographs of dried samples of **59** (B), **60** (C) and **62** (D). Adapted from ref. [48] with permission from the Royal Society of Chemistry.

The same year, Rodríguez and coworkers also reported the mononuclear derivatives containing the water soluble phosphane triphenylphosphine-3,3',3''-trisulfonic acid trisodium salt (TPPTS) and either 4-ethynylpyridine (**64**) or a propargyloxycoumarin group (**65**), as well as the dinuclear gold(I) complexes with a propargyloxycoumarin moiety and either PTA (**66**) or DAPTA (**67**) [49]. Compound **64** self-assembled in water, giving rise to micrometric fibrillary structures. On the other hand, complex **65** was highly soluble in water and small aggregates could be only detected in DLS experiments. The different behavior between **64** and **65** pointed out the importance of the ethynylpyridine unit in the directionality of the aggregation process. In the case of the dinuclear complexes, a different pattern was also observed. Thus, **66** presented rod-like structures with length around 3  $\mu\text{m}$ , whereas in **67**, smaller spherical aggregates of ca. 100 nm were observed, which was attributed to the higher steric hindrance of the DAPTA phosphane in front of PTA. All the complexes showed in solution emission assigned to the chromophoric organic ligand and in the case of the coumarin derivatives, the nuclearity of the complexes was determinant on observing room temperature fluorescence (**65**) or phosphorescence (**66** and **67**), due to the more favorable intersystem crossing in the gold(I) dinuclear complexes.

Alkynyl gold(I) complexes containing PTA and DPTA phosphanes and the chromophores terpyridine (**68**, **69**) and bipyridine (**70**, **71**), were reported by Rodríguez, Lima and coworkers in 2018 [50]. The complexes were able to self-assemble in water and DMSO, through two different assembly modes according to a detailed NMR analysis, which was supported by density functional theory calculations: (i) chain assemblies through aurophilic interactions; and (ii) stacked assemblies, which are based on Au- $\pi$  and  $\pi$ - $\pi$  interactions (Figure 26). The initial aggregates were of nanometric size as confirmed by DLS and SAXS experiments and merged to long fibers over time in a process promoted in

water. The different supramolecular environments were reflected in the optical properties of the aggregates. Thus, in pure DMSO, the compounds presented blue emission with a band centered at 430 nm and was assigned to the singlet metal-to-ligand charge-transfer ( $^1\text{MLCT}$ )/singlet ligand-to-ligand charge-transfer ( $^1\text{LLCT}$ ) transition. This band slightly red shifted in the presence of small water contents and in pure water a new broad band centered at ca. 630 nm appeared which was attributed to the presence of excimers due to  $\pi-\pi$  or  $\text{Au}-\pi$  interactions that seemed to be more favored in this solvent.

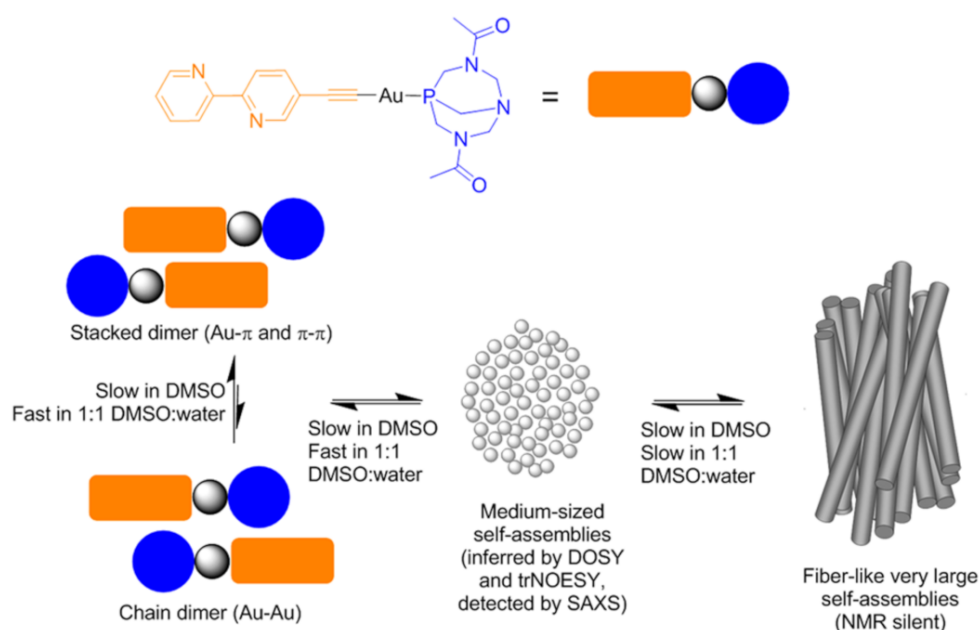


**Figure 26.** Schematic representation of the possible aggregates observed in solution for complexes 68–71 and exemplified in the illustration for 71. Reprinted with permission from ref. [50]. Copyright 2018 American Chemical Society (further permissions related to the material excerpted should be directed to the ACS).

Several alkynyl gold(I) isocyanide complexes that form large luminescent self-assemblies have been reported in recent years (Figure 27). In these complexes, the linearity imposed by the Au(I) coordination together with the linearity of both ligands is very attractive for the formation of highly ordered structures. In 2017, Yam and coworkers reported the tetranuclear alkynyl gold(I) isocyanide complexes 72–75 [51]. The self-assembly of the complexes upon incorporation of a poor solvent such as methanol to dichloromethane solutions was monitored by means of UV-vis absorption, emission,  $^1\text{H-NMR}$  and DLS studies. Upon aggregation, the emission of 72 changed from green to orange-red, due to the decrease of the emission centered at ca. 479 nm and was assigned to a LLCT transition of the monomer, and a subsequent increase of the emission at ca. 674 nm was assigned to aggregates formed by means of auophobic interactions, with the participation of  $\pi-\pi$  stacking and hydrophobic interactions of the calixarene units. Similar emission changes were observed also for 73–75 although to a lesser extent, which was attributed to a lower degree of aggregation, due to the higher polarity of these complexes and consequently their higher solvation in MeOH. Electronic microscopy analysis allowed for visualizing the morphology of the aggregates in the presence of different contents of MeOH. The formation of micellar structures with a diameter around 180 nm was detected for samples of 72 with 50% of MeOH content. Additional increase of this solvent gave rise to the interconnexion of the micellar structures and, finally, to less uniform fibrillar networks (Figure 28). The authors, due to the surfactant-like structure of the complex, tentatively explained this aggregation behavior, with the hydrophobic tert-butyl groups on one side of the molecule and the polar oligoether units on the opposite side. So, upon addition



of MeOH, self-assembly assisted by aurophilic interactions and other noncovalent forces occurred in order to minimize the contact between the apolar groups and the polar solvent.

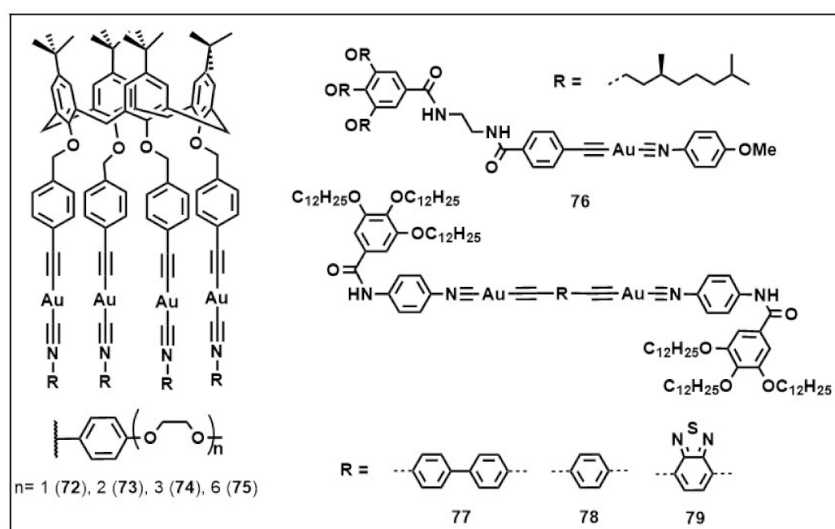


**Figure 27.** Alkyne-gold(I)-isocyanide complexes that form large luminescent supramolecular assemblies.

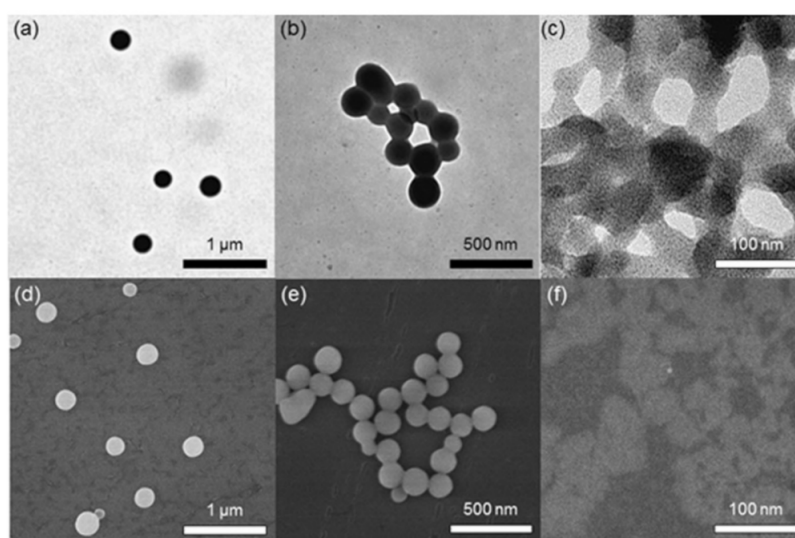


**Figure 28.** TEM (top) and SEM (bottom) images of **72** ( $1.5 \times 10^{-5}$  M) in: (a,d) 50%, (b,e) 70%, and (c,f) 90% MeOH/CH<sub>2</sub>Cl<sub>2</sub> mixture. Reproduced with permission from ref. [51]. Copyright 2017 John Wiley and Sons.

The same year, the alkyne-gold(I)-isocyanide metallogelator **76** was reported by Wang et al. [52]. The complex was able to form a reversible supramolecular gel in an apolar methylcyclohexane/CHCl<sub>3</sub> (95:5, v:v) solution (Figure 29A). The gel presented cyan triplet emission with a maximum located in 479 nm and a shoulder peak at 513 nm, which was attributed to the establishment of aurophilic interactions. TEM images revealed the presence of crosslinked fibers of several microns' length and around 100 nm width (Figure 29B). Small-angle X-ray diffraction (XRD) analysis indicated that **76** is arranged in the fibers following a lamellar pattern. A detailed mechanistic study conducted by means temperature-variable UV-vis absorption experiments as well as <sup>1</sup>H-NMR measurements determined that the self-assembly process is co-driven by Au(I)⋯Au(I) interactions and hydrogen bonding involving the amide groups of the complex, following a nucleation–elongation cooperative mechanism.



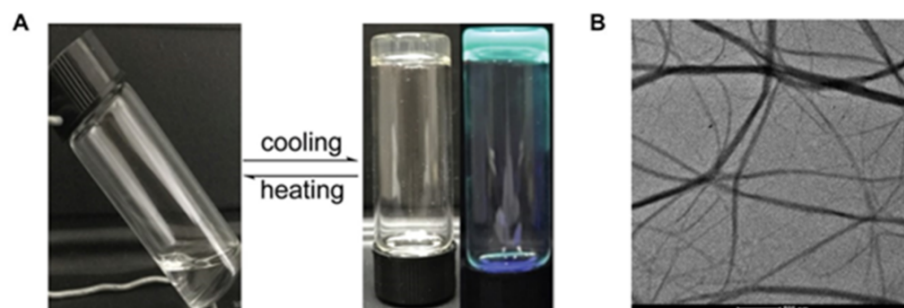


**Figure 29.** (A) Thermo-responsive sol-gel transition behavior of **76**. Cyan emission was observed by irradiating the gel with a 365 nm UV lamp; (B) TEM micrograph of **76** (copper grid, 0.40 mM of **76** in MCH/CHCl<sub>3</sub> (95:5, *v/v*) solution). Adapted from ref. [52] with permission from the Royal Society of Chemistry.

Dinuclear alkynyl gold(I) isocyanide complexes **77–79** were reported by He and co-workers in 2020 [53]. The compounds presented different central conjugated moieties which influenced their self-assembly and photophysical properties. The three compounds presented good solubility in CHCl<sub>3</sub> whereas it is aggregated in highly apolar solvents such as methylcyclohexane, hexane and heptane. In concrete, **77** and **79**, having larger conjugated central units, were able to form one-dimensional fibers and gels, whereas **78**, with a small central chromophore, formed spherical micelles (Figure 30). The different behavior was attributed to stronger  $\pi$ - $\pi$  interactions in **77** and **79**, which in combination with other intermolecular forces such as aurophilic interactions and hydrogen bonding were responsible of the self-assembly process. Photophysical studies revealed that aggregated samples of **77** and **78** displayed strong yellowish phosphorescence which was attributed to triplet ligand centered  $\pi \rightarrow \pi^*$  transition with the involvement of Au(I)⋯Au(I) interactions. On the other hand, for **79**, having a central heterocyclic aromatic unit, only quenching of the monomeric emission was observed upon aggregation.

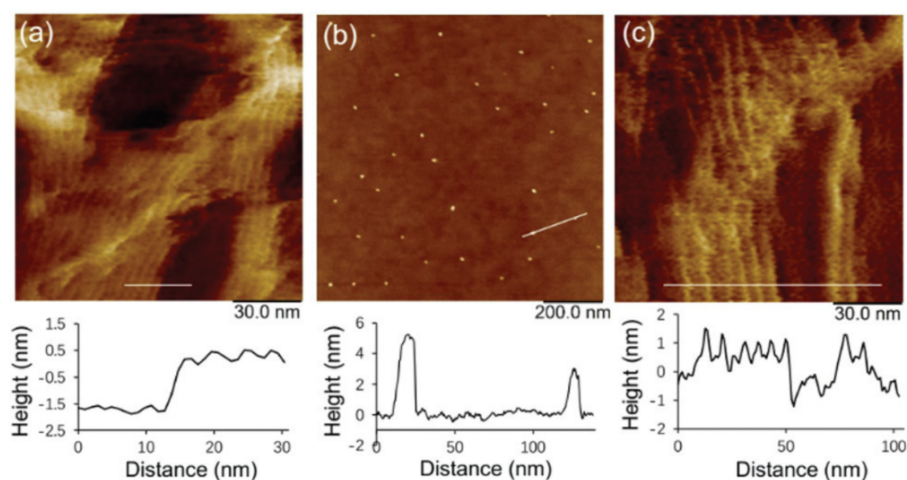


**Figure 30.** AFM images of the self-assembled nanostructures of (a) **77** in heptane solution, (b) **78** in MCH solution and (c) **79** in MCH solution, as well as their height profiles after solvent evaporation. Reproduced from ref. [53] with permission from the Royal Society of Chemistry.

Other miscellaneous gold chemical structures studied in the last years are shown in Figure 31. In 2018, López-de-Luzuriaga and coworkers reported the adeninate gold(I) complex **80** [54]. The complex was able to form a supramolecular luminescent hydrogel at unexpected high concentrations (250 mM). The driving forces of the assembly were aurophilic interactions and hydrogen bonding according to the X-ray crystal structure analysis which revealed Au<sup>I</sup>⋯Au<sup>I</sup> distances of 3.2081(6) Å in the solid state. Moreover,

both types of interactions presented comparable strength, as determined by computational analysis. Electronic microscopy investigations of the xerogel revealed that the complex self-assembled into ultrathin nanowires of  $5.3 \pm 1.9$  nm of diameter and up to  $1.5 \mu\text{m}$  in length (Figure 32). Luminescent studies in more diluted concentrations showed a red shift of the excitation (293–325 nm) and emission (415–440 nm) in the concentration range 0.25–5.0 mM which was compatible with the formation of oligomers in solution through  $\text{Au(I)} \cdots \text{Au(I)}$  interactions. Oligomers composed by 2–12 molecules (concentration range 5.0–100 mM) was also detected by means of pulsed-gradient spin–echo NMR experiments.

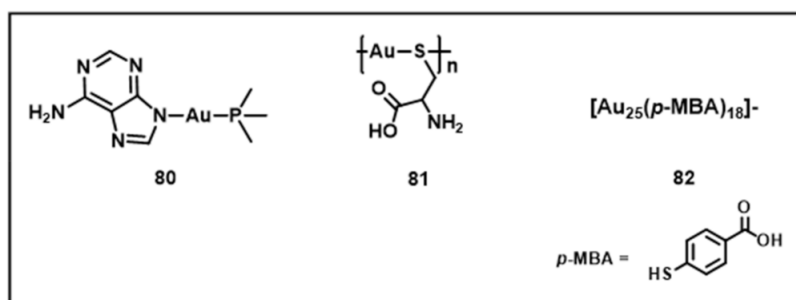


Figure 31. Miscellaneous chemical structures that self-assemble via aurophilic interactions.

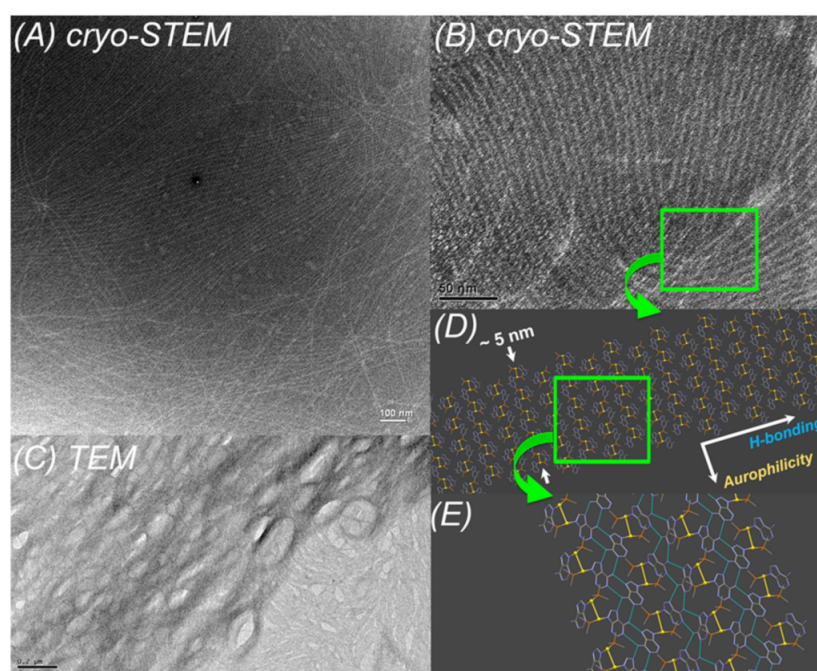
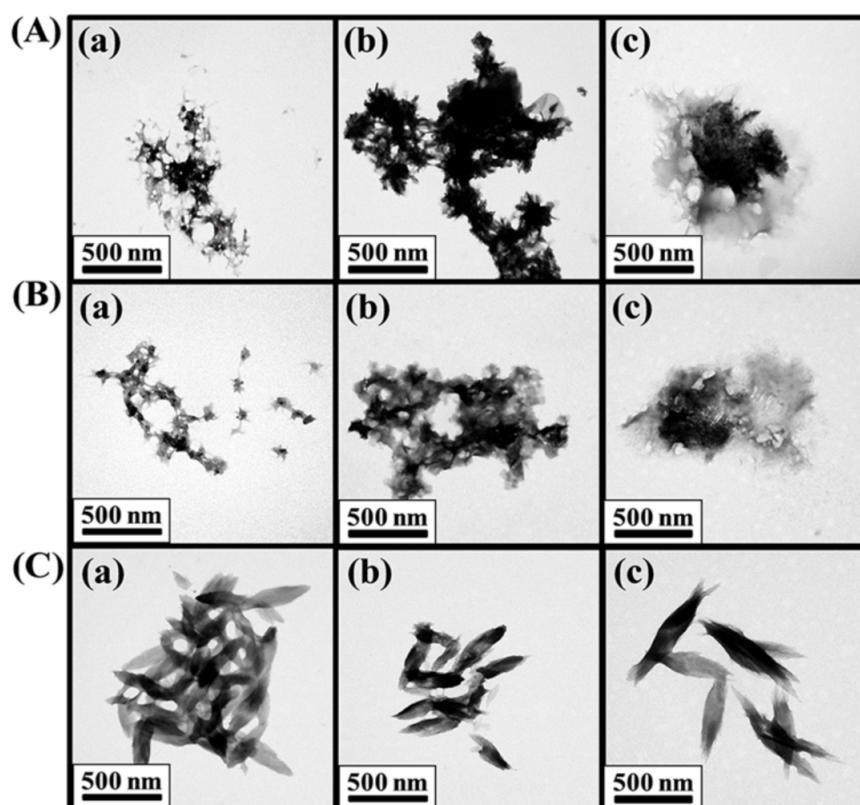


Figure 32. Cryo-STEM (A,B) images, TEM (C) image and proposed morphology of the UNWs of **80** based on its X-ray crystal structure (D,E). Reprinted with permission from ref. [54]. Copyright 2018 American Chemical Society.

Hybrid systems  $\text{Au NCs}/-[\text{Cys-Au(I)}]_n-$ , composed by Au nanoclusters (Au NCs) embedded in aggregated coordination polymers **81** ( $-[\text{Cys-Au(I)}]_n-$ ) were reported by Chang, Huang et al. in recent years [55,56]. ( $-[\text{Cys-Au(I)}]_n-$ ) polymers were prepared easily by reaction between  $\text{HAuCl}_4$  and cysteine (Cys) in mildly acidic to neutral pH values. Interestingly, when pure D- or L-Cys enantiomers were used, the polymers self-assembled at  $\text{pH} \leq 7$  into supramolecules with irregular morphologies larger than 500 nm (Figure 33A,B), which showed strong absorption in the near-UV region and chiroptical properties due to the formation of helically chiral structure. The self-assembly process was driven by hydrogen bonding, zwitterionic interactions and  $\text{Au(I)} \cdots \text{Au(I)}$  interactions.

On the other hand, when mixtures of D/L-Cys were employed to prepare the polymers, spindled-shaped aggregates with no chiroptical properties were obtained (Figure 33C). Partial reduction of  $-\text{[D-Cys-Au(I)]}_n-$  and  $-\text{[L-Cys-Au(I)]}_n-$  conducted to the formation of the hybrid systems Au NCs/ $-\text{[D-Cys-Au(I)]}_n-$  and Au NCs/ $-\text{[L-Cys-Au(I)]}_n-$ , which presented a red long-lived luminescence (630 nm). This emission was attributed to the highly dense and rigid Cys-Au(I) complexes on the surface of the Au(0) core and was assigned to a LMMCT origin where aurophilic interactions were coupled with ligand-ligand interactions. The as-formed Au NCs/ $-\text{[D-Cys-Au(I)]}_n-$  and Au NCs/ $-\text{[L-Cys-Au(I)]}_n-$  were successfully employed as a nanomatrix for surface-assisted laser desorption/ionization mass spectrometry (LDI-MS) for D-carnitine and L-carnitine, respectively.



**Figure 33.** TEM images of the products from the reactions of  $\text{HAuCl}_4$  (0.7 mM) with (A) L-Cys (5.0 mM), (B) D-Cys (5.0 mM), and (C) the mixture of L-Cys (2.5 mM) and D-Cys (2.5 mM) for 1 h in sodium phosphate solutions (10 mM) at pH values of (a) 3, (b) 5 and (c) 7. Adapted with permission from ref. [56]. Copyright 2018 American Chemical Society.

Self-assembly of gold nanocluster **82** via  $\text{Au(I)}\cdots\text{Au(I)}$  interaction was reported by Xie, Yao et. al in 2019 [57]. The self-assembly process was promoted by cyclic dialysis, which induced the transformation of the initial  $[\text{Au}_{25}(\text{SR})_{18}]^-$  NC to a NC building block containing longer  $\text{SR-}[\text{Au(I)-SR}]_x$  motifs ( $x > 2$ ) and a smaller Au(0) core. This transformation enriched the content of Au(I) species in the protecting shell and hence increased the directed aurophilic interactions between neighbors' nanoclusters. This intermolecular bonding, together with  $\pi$ - $\pi$  interactions, drove the self-assembly of the nanoclusters into well-defined luminescent nanoribbons in solution. The system presented two emission bands: i) a higher energy transition band at 483 nm, only observable at very low temperatures, which is assigned to intraligand or metal-perturbed intraligand phosphorescence originated from  $\pi$ - $\pi$  stacking; and ii) a lower energy band which red-shifted from ca. 600 nm (77 K) to 655 nm (298 K) when increasing temperature and attributed to triplet states with ligand-to-metal-metal charge transfer (LMMCT) character.



## 4. Modulation of Luminescent Supramolecular Assemblies Based on the Presence of Cations and Anions

### 4.1. Detection of Metal Ions Based on the “On”-“Off” Switching of Au(I)⋯Au(I) Intramolecular Interactions

In 1998, Yam et al. reported on the chemosensing of potassium ions based on the “turned on” of aurophilic interactions in dinuclear gold(I) complexes functionalized with a benzo-crown thiolate [58]. In the presence of potassium ions, the aurophilic interactions were generated in situ which resulted in changes in the luminescence properties of the compounds in solution. After this pioneering work, several studies based on the same strategy have been reported to develop gold(I) chemosensors of metal ions. In the last five years, the group of Yam et al. has developed new alkynyl gold(I) complexes containing crown ether and calixarene moieties. Thus, in 2017, Yam’s group reported the crown ether-containing gold(I) derivatives **83–88** (Figure 34) and studied their binding properties towards  $K^+$  [41]. The spectral changes (UV-vis absorption and emission) observed for  $CH_2Cl_2/CH_3CN$  solutions of **83–85** upon titration with  $K^+$ , indicated a 1:1 binding mode. The most pronounced changes in the emission spectra were observed for compound **83**, with a remarkable increase of the low energy band at about 613 nm, which was ascribed to switching “on” of aurophilic interactions upon the binding of the potassium ion in a sandwich-binding mode. The changes observed in  $^1H$ -NMR experiments were also in agreement with a sandwich conformation of the complex upon association with potassium. A similar increase of the low energy emission band (603 nm) upon addition of  $K^+$  was observed for **86** also suggesting the establishment of aurophilic interactions. For this complex, containing a long oligoether chain, which could also interact with the metal ion, a 1:2 binding mode was found. For complex **87**, containing a naphthalene rigid bridging unit, the interaction with potassium gave rise to a decrease of the low energy band, which was attributed to the disruption of aurophilic interactions present in the original complex upon binding with the metal ion. Complex **88** presented a crown ether moiety too large for an efficient interaction with  $K^+$ , however, experiments with larger  $Cs^+$ , showed an increase of the low energy band about 609 nm upon addition of this cation, indicating that the binding of  $Cs^+$  could lead to Au(I)⋯Au(I) interactions.

Yam and co-workers also reported several alkynyl[4]calixarene-gold(I) complexes as chemosensors of diverse metals in 2017 [51]. They used complexes **72–75** (Figure 27) whose self-assembly behavior has been commented in the previous section, as well as complexes **89–92** (Figure 34) to study the host-guest interactions involving several metal ions. Interaction with the cations gave rise to an important enhancement of a red-orange emission above 600 nm, which was assigned to an excited state originating from the enhanced aurophilic interactions. All the complexes showed a great affinity for group 13 ions with binding constants ( $K_s$ ) in the order of  $10^6 M^{-1}$  and detection limits around 0.1  $\mu M$ . Particularly, complex **90** exhibited a high selectivity towards  $In^{3+}$  in front of other metal ions, even in front of  $Al^{3+}$ , which belongs to the same 13 group.  $^1H$ -NMR experiments indicated that the binding of  $In^{3+}$  occurred the lower rim of the calix[4]arene ligand, as illustrated in Figure 35.

In 2018, Yam and coworkers reported the polyamide-containing alkynyl gold(I) complex **93** (Figure 34) [59]. The amide units made the complex suitable for the recognition of  $Cd^{2+}$  ions. Binding of the metal ion to the complex in  $CH_2Cl_2/CH_3CN$  solutions provoked an enhancement of high-energy emission band of the complex at ca. 450 nm, which was attributed to the suppression of photo-induced electron transfer (PET) process of the o-phenylenediamine unit and rigidification of the molecules. On the other hand, the binding also resulted in a slight decrease of the low energy emission band at ca. 650 nm, which was associated with the presence of intramolecular Au(I)⋯Au(I) interactions previously given the addition of the metal. These interactions were disrupted upon association of  $Cd^{2+}$  to the gold(I) complex. The binding process was additionally confirmed by means of UV-vis absorption, ESI-MS and  $^1H$ -NMR experiments.

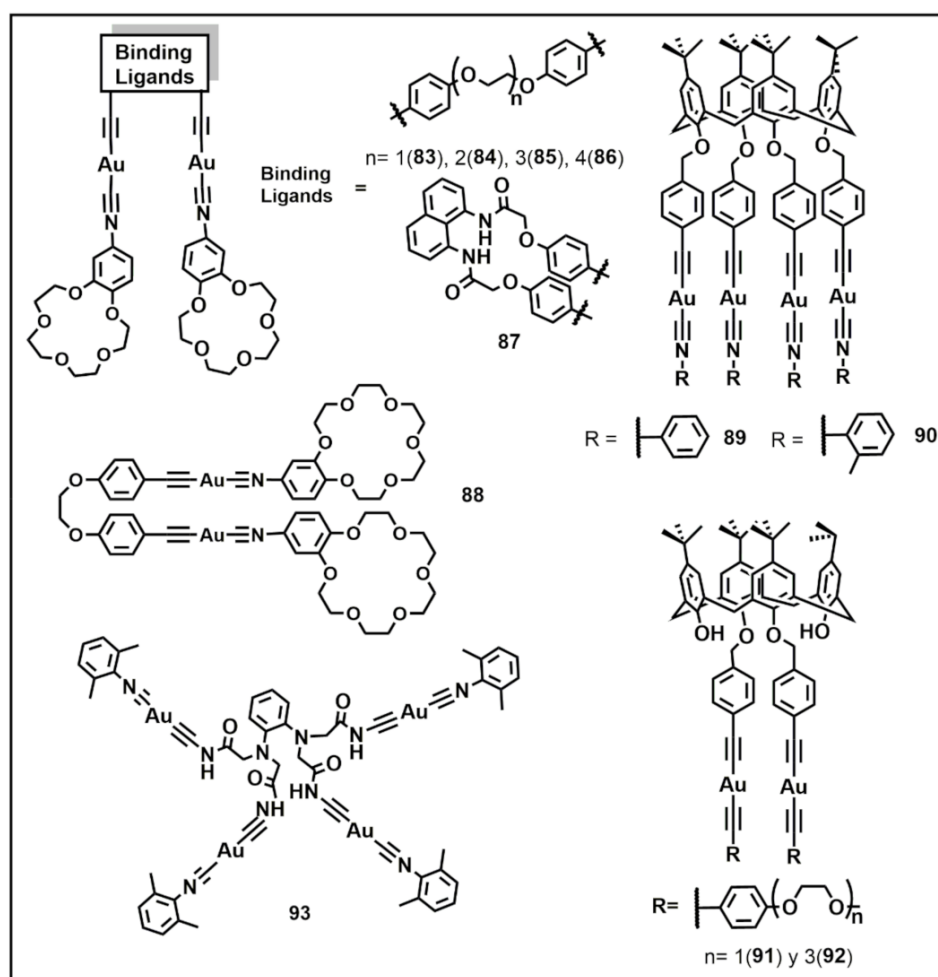


**Figure 34.** Gold(I) complexes used in the detection of ion metals via the "on"- "off" switching of auriphilic intramolecular interactions.

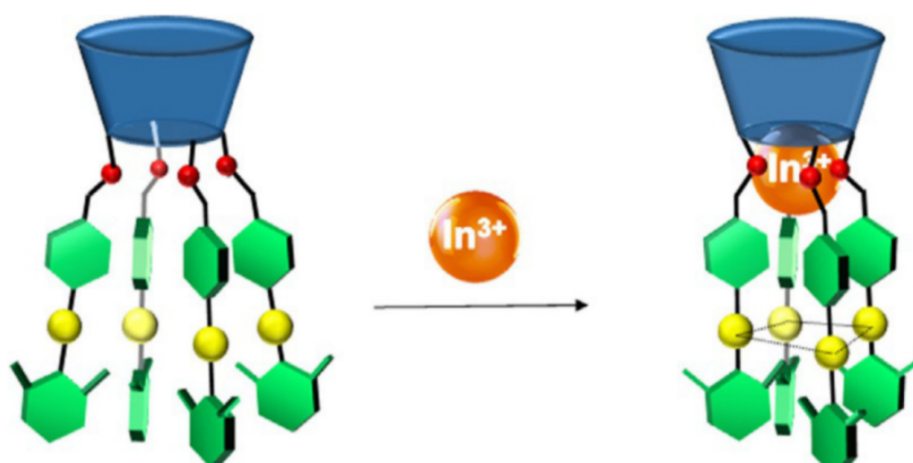


**Figure 35.** Schematic drawing of the proposed binding mechanism of complex 90 with  $In^{3+}$  ion. Adapted with permission from ref. [51]. Copyright 2017 John Wiley and Sons.

#### 4.2. Assembly/disassembly Processes Based on the Interaction of Gold(I) Complexes with Other Species

Several cations and anions have been used to promote or disrupt supramolecular assemblies involving gold(I) complexes. Special attention has been paid in the last years



to the use of cations to induce aggregation and, most frequently, disaggregation of gold(I) supramolecular assemblies.

As commented previously, complex **36** (Figure 16) presents interesting AIE properties. Due to its efficient emission in the aggregated state, this compound was also explored as a chemosensor for different metal ions [34]. The complex showed a high selectivity towards  $\text{Hg}^{2+}$  in  $\text{CH}_3\text{CN}:\text{H}_2\text{O}$  (1:1, v:v). Upon addition of the metal, the emission of the aggregated complex at 575 nm experienced a drastic decrease, caused by the depolymerization of the complex due to the coordination with  $\text{Hg}^{2+}$ . DLS experiments additionally demonstrated that the binding process reduced the particle size (from 955 nm to 396 nm) and hence the aggregation upon addition of 1 equivalent of  $\text{Hg}^{2+}$ .

The supramolecular self-assemblies of **68–71** (Figure 22) were also disrupted upon coordination of the terpyridine and bipyridine units of the complexes to  $\text{Zn}^{2+}$  [50]. Thus, upon coordination with the metal ion, the red emission assigned to the aggregates disappeared whereas a strong blue fluorescence was assigned to  $^1\text{MLCT}$ , rose. Interestingly, the authors demonstrated the reversibility of the aggregation process by adding a  $\text{Zn}^{2+}$  encapsulating agent ((1,2-[bis(3-aminopropyl)amine]-ethane or 4,7,13,16,21,24-hexaoxa-1,10-diazabicyclo[8.8.8]-hexacosane cryptand), which provoked the reappearance of the red emission associated with the aggregates. The disaggregation/aggregation process was also confirmed by means of  $^1\text{H-NMR}$  experiments in  $\text{D}_2\text{O}$  and SAXS analysis, in the presence of  $\text{Zn}^{2+}$  followed by the addition of the encapsulating agent.

Disruption of the supramolecular organogel formed by **76** (Figure 27) was observed upon addition of  $\text{AgOTf}$  [52]. It was rationalized by the authors and confirmed by IR analysis that  $\text{Ag}^+$  could interact with the acetylide units of **76**, which affected to the distance of the stacked neighboring monomers with the consequent breakup of the supramolecular gel. Subsequent addition of tetrabutylammonium iodide restored the gel and the initial cyan emission, by precipitation of  $\text{AgI}$  salt (Figure 36).

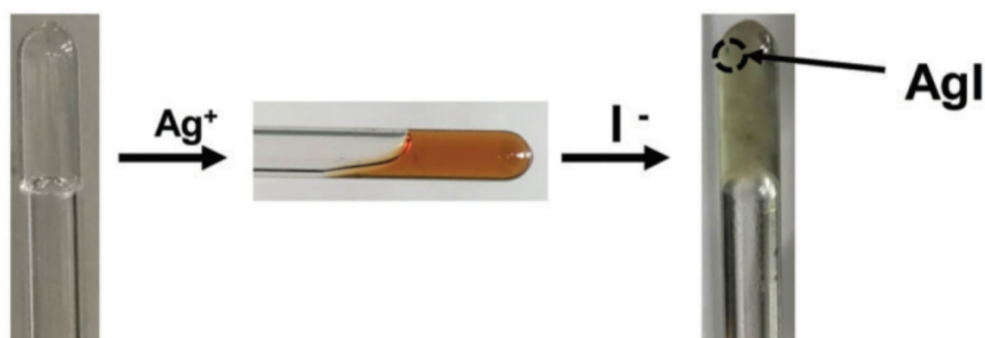


**Figure 36.** Reversible sol–gel transition of **76** via the successive addition of  $\text{AgOTf}$  and  $\text{Bu}_4\text{NI}$ . Adapted from ref. [52] with permission from the Royal Society of Chemistry.

The interaction between complex **78** (Figure 27) and  $\text{Ag}^+$  was also investigated [53]. UV-vis absorption and emission titrations were carried in a good solvent for both species, avoiding in this way an initial aggregated state for **78**. The luminescence changes revealed two steps in the binding process involving  $\text{Ag}^+$  and the gold(I) complex. Upon addition of  $\text{Ag}^+$  up to 1 equivalent, a new band at ca. 570 nm gradually appeared, which, according to the authors, could be related with the switching “on” of aurophilic interactions in a sandwich binding mode of the silver ions (Figure 37). Further increase of the silver(I) content gave rise to the disappearance of the emission band, pointing out the dissociation of the 1:2 sandwich type complex and formation of the 1:1 complex involving ions  $\text{Ag}^+$  and the alkynyl groups of **78**.

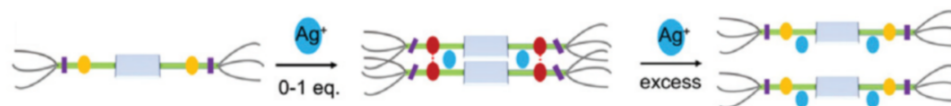


**Figure 37.** Schematic representation for  $\text{Ag}^+$  binding of 78. Adapted from ref. [53] with permission from the Royal Society of Chemistry.

Aggregation induced emission of gold(I)-cysteine polymers (81, Figure 31), using its interaction with  $\text{Ca}^{2+}$ , was achieved by Pei and co-workers in 2015 [60]. Oligomeric Au(I)-cysteine complexes were not emissive in solution, however, upon addition of  $\text{Ca}^{2+}$ , the divalent metal coordinated to the cysteine moieties, inducing the crosslinking between the oligomers and giving rise to luminescent dense aggregates. The strong emission at 615 nm was attributed to the establishment of  $\text{Au(I)}\cdots\text{Au(I)}$  within the dense aggregates. The crosslinking process was very selective towards  $\text{Ca}^{2+}$  (Figure 38) and was not detected for other divalent cations under the same conditions.

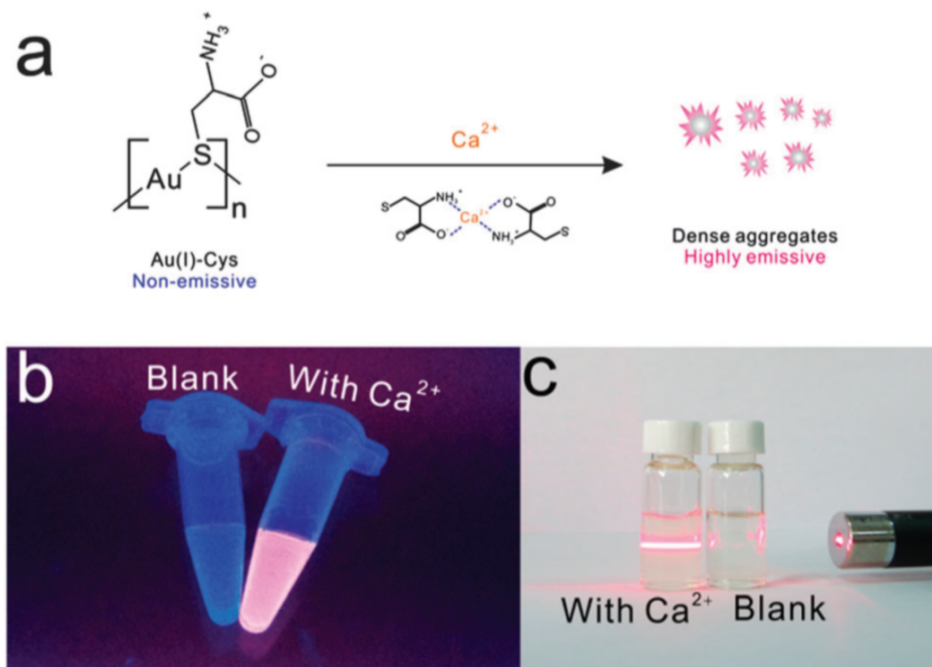


**Figure 38.** (a) Schematic representation of the detection of  $\text{Ca}^{2+}$  based on the AIE property of Au(I)-cysteine oligomers; (b) pictures of 81 in the absence and presence of  $\text{Ca}^{2+}$  under UV light; (c) Rayleigh scattering test using a red laser pointer. Reproduced from ref. [60] with permission from the Royal Society of Chemistry.

In 2016, studies performed by Iwamura et al. demonstrated that the addition of tetraalkylammonium cations to dicyanoaurate solutions (94, Figure 39) promoted the oligomerization of the gold(I) complex [61]. Absorption and emission measurements revealed that tetraalkylammonium cations stabilized larger aggregates both in the ground state and in the excited state. In the case of the emission spectra, the phosphorescence band was red-shifted to ca. 460 nm, indicating the presence of dicyanoaurate tetramers or larger oligomers. The emission quantum yields were also drastically increased due to the stabilization of the oligomers by  $\text{R}_4\text{N}^+$  in the excited state. This stabilization was related with the establishment of hydrophobic interactions between the tetraalkylammonium cations and CN ligands, which suppressed the dissociation of the excited-state oligomers.

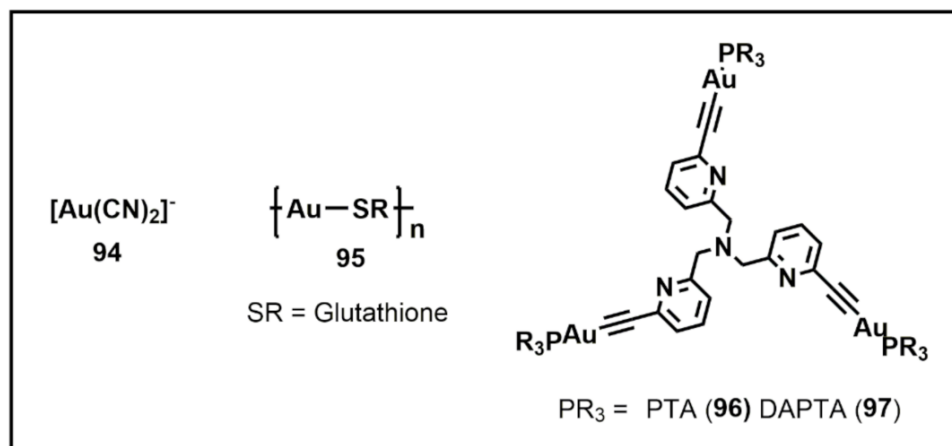


**Figure 39.** Miscellaneous chemical structures of gold(I) complexes that participate in assembly/disassembly processes involving cations.

Kuroiwa and coworkers reported the interaction between dicyanoaurate **94** and steroidal alkaloid glycosides (SAGs) in 2018 [62]. Several aggregated morphologies were detected by TEM analysis, dependent on the structure of the SAGs molecule. UV-vis absorption and emission studies demonstrated that  $[\text{Au}(\text{CN})_2]^-$  showed a greater tendency to aggregate in the presence of SAGs molecules containing a protonated amino group, due to electrostatic interactions between the amine segment of the steroid and the anionic  $[\text{Au}(\text{CN})_2]^-$ . In the case of the emission, higher intensities and red-shifts of the phosphorescence band were observed, which indicated not only a higher oligomerization but also that some non-radiative relaxation processes were avoided upon interaction of the  $[\text{Au}(\text{CN})_2]^-$  oligomers with this type of SAGs.

In 2019, Zhang, Qi et al. reported the aggregation induced emission of Au(I)-glutathione (GSH) complexes (**95**, Figure 36) in the presence of  $\text{Pb}^{2+}$  [63]. Addition of the divalent metal to Au(I)-glutathione solutions resulted in highly emissive aggregates, due to the strong coordination between  $\text{Pb}^{2+}$  and the glutathione units and consequent crosslinking between gold(I) complexes, which favored the establishment of aurophilic contacts. The system was used to design a fluorometric method for the detection of sulfate-reducing bacteria (SRB), which produce sulfide. Thus, in the presence of sulfate, the bacteria generated sulfide which gave rise to the formation of  $\text{PbS}$  precipitate and drastically decreased the emission of the Au(I) aggregates at 575 nm (Figure 40).

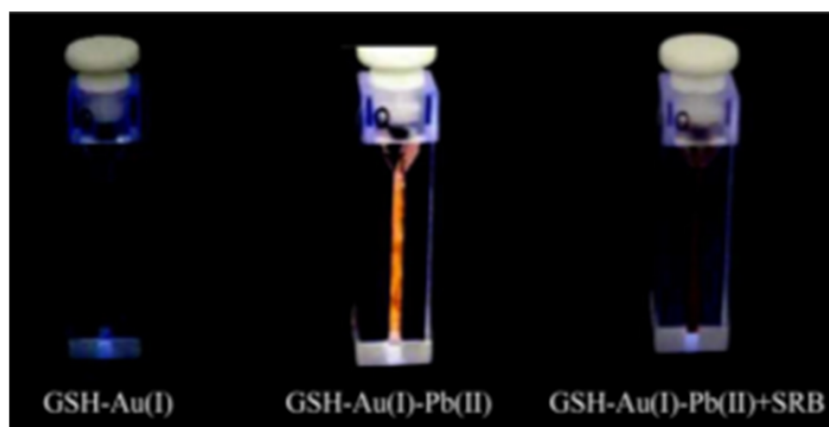


**Figure 40.** Pictures under UV-light of solutions containing GSH-Au(I) complexes, GSH-Au(I)-Pb(II) complexes and GSH-Au(I)-Pb(II) complexes + SRB bacteria. Adapted with permission from ref. [63]. Copyright 2019 Springer Nature.

In 2020, Rodriguez, Licini and co-workers reported the interaction between the tripodal gold(I) polypyridyl complexes **96–97** (Figure 36) and the metallic cations  $\text{Cu}^+$  and  $\text{Zn}^{2+}$  [64]. Before the addition of the cations, the gold(I) complexes were aggregated in solution as indicated by their absorption and emission spectra. The complexes presented an emission band with maximum at ca. 550 nm, which was assigned to triplet metal-perturbed intraligand  $\pi-\pi^*$  ( $\text{C}\equiv\text{C}$ ) transitions or  $^3\text{MMLCT}$  transitions, with M-M contacts corresponding to intra- and intermolecular aurophilic interactions. Upon addition of the metal cations, a progressive decrease on the absorption baseline was observed, which was indicative as of disaggregation of the Au(I) complexes. In the case of the emission spectra, a progressive quenching of the emission at 550 nm was detected, indicating the interaction between the gold(I) complexes and Cu(I) and Zn(II), respectively. The interaction mechanism was analyzed by means of NMR and IR experiments and revealed different coordination sites for every metal. Thus, Zn(II) coordinated to the nitrogen atoms of the polypyridyl group, whereas Cu(I) coordinated preferentially to the alkynyl groups.

The use of anions to modulate the assembly/disassembly of gold(I) has been much less explored. The interaction between the alkynyl gold(I) phosphanes **54–55** (Figure 22) and anions was investigated by Rodriguez et al. in 2018 [65]. In particular, the authors studied the molecular recognition of two phosphate-containing molecules, namely sodium hexametaphosphate (HMP) and a single-stranded 24-long oligonucleotide, using UV-vis absorption spectroscopy, DLS and microscopy techniques. As commented previously, **54** and **55** self-assemble in water to give rise to the formation of very fibers. This aggregation starts with the formation of small spherical aggregates in fresh solutions, which act as nucleation points [45]. In this work, it was observed that the interaction with HMP gave rise to the formation of larger spherical aggregates in the initial stages of aggregation, as confirmed by means of DLS and microscopy analysis. UV-vis absorption spectra indicated that HMP favored the formation of aurophilic interactions and  $\pi-\pi$  head-to-tail interactions, which was in agreement with the formation of larger aggregates. On the other hand, interaction with the nucleotide provoked a remarkable different effect. Microscopy analysis indicated the formation of smaller aggregates and UV-vis measurements were compatible with a decrease in the contribution of the aurophilic contacts and an arrangement of the gold(I) molecules in the aggregates in a head-to-head conformation, which could be induced by the interaction with the anionic linear nucleotide.

In 2020, Moro and co-workers reported the interaction between the naphthyridine-ethynyl-gold(I) complex **98** (Figure 41) and several guanosine nucleotides [66], in a molecular recognition process based on the formation of multiple hydrogen bonding between the naphthyridine unit and the guanosine nucleotides. Complex **98** exhibited aggregation induced emission in water, and at high concentrations presented to emission bands, a higher energy band at ca. 450 nm, assigned to the gold(I) monomer and a lower energy band at ca. 550 nm assigned to gold(I) aggregates. The presence of aggregates with a size of ca. 60 nm was further confirmed by means of SAXS analysis. The interaction with guanosine nucleotides (mono-, di- and triphosphate) provoked in all cases a decrease in the emission of the aggregates and an increase in the emission of the monomer, indicating that the formation of hydrogen bonds involving the naphthyridine moiety and the nucleotides gave rise to the disruption of intermolecular aurophilic bonds present in the aggregates.

Bu and coworkers reported recently the interaction between the cationic gold(I) complexes **99–100** (Figure 41) and several anionic block copolymers [67,68]. The electrostatic interaction between the gold(I) complexes and poly(styrene-co-acrylate sodium) and poly(ethylene oxide-co-acrylate sodium) block copolymers gave rise to the formation of brightly luminescent micelles. The blue emission (ca. 475 nm) was especially strong in the case of **99** and was related to the establishment of aurophilic interactions in the micellar core. Micelles obtained by the assembly of **99** with poly(ethylene oxide-co-acrylate sodium) block copolymer, with a hydrodynamic diameter of 63 nm in water, were used as a luminescence bioimaging probe in living cells. Confocal laser microscopy analysis revealed that the micelles internalized easily in the cytosol of HepG2 cells [67]. Combination of

**99** with the chiral poly(ethylene glycol)-block-poly-(L-glutamic sodium) (PEG<sub>n</sub>-b-PLGS<sub>m</sub>) gave rise to the formation of worm-like micelles (Figure 42) that further aggregated to produce fiber-like gold(I)-polymer composites. It was observed a gradual increase of the phosphorescence intensity (ca. 475 nm) and quantum yield upon increasing the molecular weight of the chiral block copolymer, which was related with an increase in aurophilic interactions occurring in the system. Interestingly, a chirality transfer and amplification from the chiral block copolymers to the gold(I) complexes was observed, which provoked a remarkable increase of the CD and CPL signals [68].

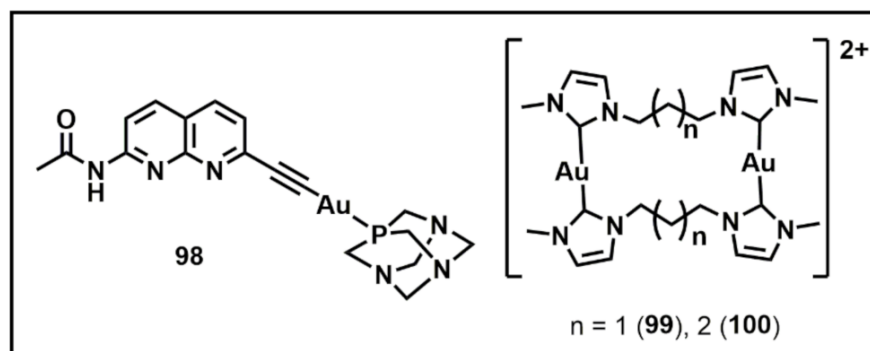


**Figure 41.** Miscellaneous chemical structures of gold(I) complexes that participate in assembly/disassembly processes involving anions.

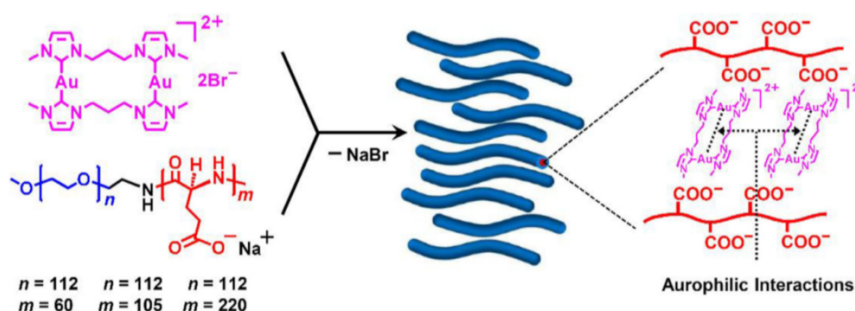


**Figure 42.** Electrostatic self-assembly of **99** with PEG<sub>n</sub>-b-PLGS<sub>m</sub> generated worm-like micelles at stoichiometric charge ratios, which further formed aggregates by hydrophilic and hydrophobic interactions. In the micellar cores of PLGS<sub>m</sub> /**99**, the intramolecular Au(I)···Au(I) interactions were evoked in water. Adapted with permission from ref. [68]. Copyright 2021 Elsevier B.V.

#### 4.3. Interaction with Luminophores

Luminescence can be introduced in non-emissive self-assemblies by means of the interaction with luminophore molecules. This was the case of the enantiomeric gold(I) complexes **101(S)** and **101(R)** (Figure 43) [69]. The complexes presented in THF/H<sub>2</sub>O 1/4 (*v/v*) an impressive dynamic hierarchical self-assembly process from vesicles to helical fibers accompanied by a chirality inversion and amplification, as revealed by in situ CD experiments. The self-assembly process was driven by  $\pi$ - $\pi$  stacking, CH···F interactions and weak aurophilic interactions (Au<sup>I</sup>···Au<sup>I</sup> distances of 3.6–3.8 Å), according to X-ray crystal structure measurements. However, although the compounds behave as typical AIEgens in THF/H<sub>2</sub>O mixtures (luminescent aggregates with non-defined shape), the hierarchical well-defined self-assemblies obtained in THF/H<sub>2</sub>O  $\frac{1}{4}$  did not exhibit luminescence (Figure 44A,B). This was achieved by co-assembling **101(R)** and **101(S)** with typical luminophores. Moreover, due to the chirality of the gold(I) complexes, circularly polarized luminescence (CPL) emerged. The enantiomers were self-assembled both with luminophores with aggregation caused quenching (ACQ), such as 9,10-bis(phenylethynyl)anthracene (BPEA), and chromophores exhibiting AIE properties, such as tetraphenyl ethylene (TPE).



In both cases, new luminescence (Figure 44C,D) and CPL signals due to the co-assembly process were detected.

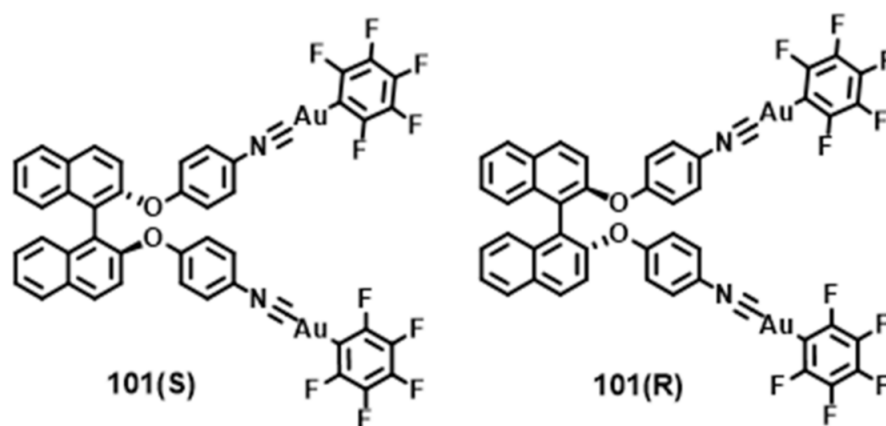


**Figure 43.** Gold(I) complexes that form luminescent supramolecular assemblies by interaction with luminophores.

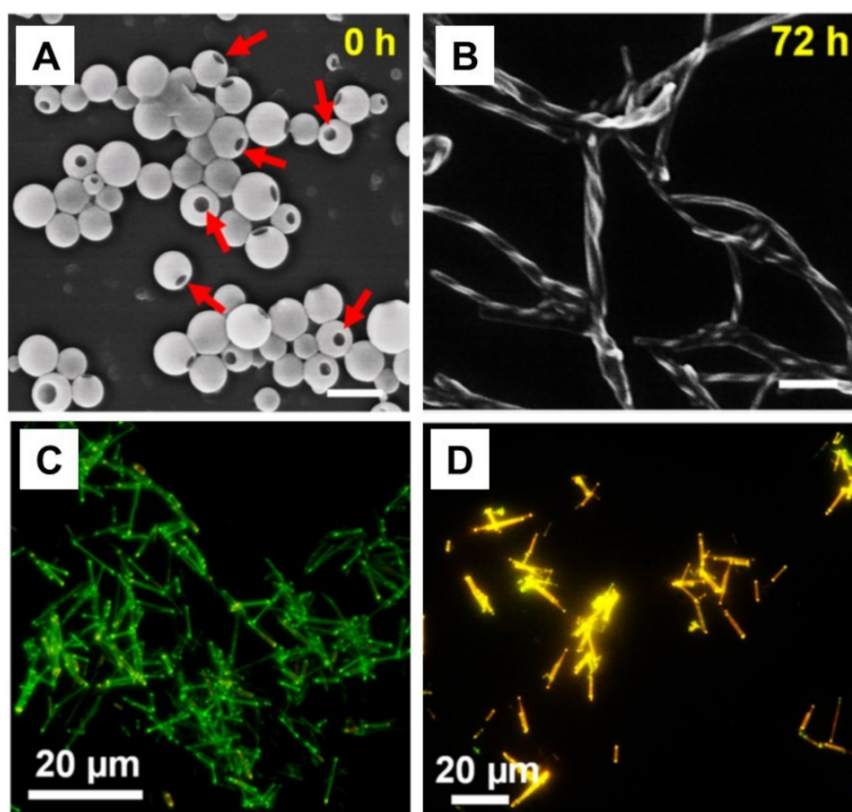


**Figure 44.** (A,B): Time-dependent SEM images to visualize the self-assembly processes of **101(R)** (THF/water: 1/4, *v/v*), corresponding to 0 h (A) and 72 h (B). (C,D): Fluorescent images of rods formed by BPEA (C) and **101(S)**/BPEA (D, co-assembly system). Adapted with permission from ref. [69]. Copyright 2019 American Chemical Society.

## 5. Conclusions

The development of luminescent assemblies in solution, based on the establishment of aurophilic interactions, is receiving increasing attention in the last years. Given the structural variability of gold(I) compounds and the fine tuning of inter- and intramolecular gold(I)⋯gold(I) interactions, together with the participation of other supramolecular forces,

a large variety of architectures with different morphological and spectroscopical properties can be built.

These assemblies have been demonstrated to be useful in a wide diversity of applications, which include the development of luminescent probes for biological purposes, the chemosensing of different species, based on the modulation of aurophilic interactions, the design of electro-optical devices such as OLEDs and CP-OLEDs, the generation of new AIE luminogens and the formation of new large supramolecular assemblies such as metallogels, vesicles and micelles, among others. The latter have potential application in different attractive areas that include the development of drug delivery systems, their use as nanoreactors and catalysts and the design of new stimuli-responsive soft materials.

**Author Contributions:** Conceptualization, R.G.; Bibliographic search and writing, G.R.-I. and R.G.; Reviewing and editing, R.G. All authors have read and agreed to the published version of the manuscript.

**Funding:** This research received no external funding.

**Acknowledgments:** Guillermo Romo-Islas acknowledges to Fundación Carolina and Secretaria de Relaciones Exteriores of Mexico for the PhD scholarship.

**Conflicts of Interest:** The authors declare no conflict of interest.

## References

1. Schmidbaur, H.; Schier, A. A briefing on aurophilicity. *Chem. Soc. Rev.* **2008**, *37*, 1931–1951. [[CrossRef](#)]
2. Schmidbaur, H.; Schier, A. Aurophilic interactions as a subject of current research: An up-date. *Chem. Soc. Rev.* **2012**, *41*, 370–412. [[CrossRef](#)]
3. Herrera, R.P.; Gimeno, M.C. Main Avenues in Gold Coordination Chemistry. *Chem. Rev.* **2021**. [[CrossRef](#)]
4. Pyykkö, P. Strong closed-shell interactions in inorganic chemistry. *Chem. Rev.* **1997**, *97*, 597–636. [[CrossRef](#)]
5. Mirzadeh, N.; Privér, S.H.; Blake, A.J.; Schmidbaur, H.; Bhargava, S.K. Innovative Molecular Design Strategies in Materials Science following the Aurophilicity Concept. *Chem. Rev.* **2020**, *120*, 7551–7591. [[CrossRef](#)]
6. Pujadas, M.; Rodríguez, L. Luminescent phosphine gold(I) alkynyl complexes. Highlights from 2010 to 2018. *Coord. Chem. Rev.* **2020**, *408*, 213179. [[CrossRef](#)]
7. Pinto, A.; Svahn, N.; Lima, J.C.; Rodríguez, L. Aggregation induced emission of gold(i) complexes in water or water mixtures. *Dalt. Trans.* **2017**, *46*, 11125–11139. [[CrossRef](#)] [[PubMed](#)]
8. Yam, V.W.W.; Au, V.K.M.; Leung, S.Y.L. Light-Emitting Self-Assembled Materials Based on d8 and d10 Transition Metal Complexes. *Chem. Rev.* **2015**, *115*, 7589–7728. [[CrossRef](#)] [[PubMed](#)]
9. Lima, J.C.; Rodríguez, L. Applications of gold(i) alkynyl systems: A growing field to explore. *Chem. Soc. Rev.* **2011**, *40*, 5442–5456. [[CrossRef](#)] [[PubMed](#)]
10. Mansour, M.A.; Connick, W.B.; Lachicotte, R.J.; Gysling, H.J.; Eisenberg, R. Linear Chain Au(I) Dimer Compounds as Environmental Sensors: A Luminescent Switch for the Detection of Volatile Organic Compounds. *J. Am. Chem. Soc.* **1998**, *120*, 1329–1330. [[CrossRef](#)]
11. Liu, Q.; Xie, M.; Chang, X.; Gao, Q.; Chen, Y.; Lu, W. Correlating thermochromic and mechanochromic phosphorescence with polymorphs of a complex gold(i) double salt with infinite aurophilicity. *Chem. Commun.* **2018**, *54*, 12844–12847. [[CrossRef](#)] [[PubMed](#)]
12. López-De-Luzuriaga, J.M.; Monge, M.; Olmos, M.E.; Quintana, J.; Rodríguez-Castillo, M. Stimuli-Responsive Solvatochromic Au(I)-Ag(I) Clusters: Reactivity and Photophysical Properties Induced by the Nature of the Solvent. *Inorg. Chem.* **2019**, *58*, 1501–1512. [[CrossRef](#)] [[PubMed](#)]
13. Lima, J.C.; Rodríguez, L. Supramolecular gold metallogelators: The key role of metallophilic interactions. *Inorganics* **2015**, *3*, 1–18. [[CrossRef](#)]
14. Zhao, Q.; Li, F.; Huang, C. Phosphorescent chemosensors based on heavy-metal complexes. *Chem. Soc. Rev.* **2010**, *39*, 3007–3030. [[CrossRef](#)]
15. Zhang, M.M.; Li, K.; Zang, S.Q. Progress in Atomically Precise Coinage Metal Clusters with Aggregation-Induced Emission and Circularly Polarized Luminescence. *Adv. Opt. Mater.* **2020**, *8*, 1–26. [[CrossRef](#)]
16. Gimeno, M.C.; Laguna, A. Chalcogenide centred gold complexes. *Chem. Soc. Rev.* **2008**, *37*, 1952–1966. [[CrossRef](#)]
17. Wang, Y.Q.; Jiang, X.F.; Li, H.; Yu, S.Y. Self-Assembly of a Au<sub>16</sub> ring via metal-metal bonding interactions. *Chem. An Asian J.* **2015**, *10*, 1146–1149. [[CrossRef](#)]
18. Yao, L.Y.; Lee, T.K.M.; Yam, V.W.W. Thermodynamic-Driven Self-Assembly: Heterochiral Self-Sorting and Structural Reconfiguration in Gold(I)-Sulfido Cluster System. *J. Am. Chem. Soc.* **2016**, *138*, 7260–7263. [[CrossRef](#)]
19. Lei, Z.; Zhang, J.Y.; Guan, Z.J.; Wang, Q.M. Intensely luminescent gold(i) phosphinopyridyl clusters: Visualization of unsupported aurophilic interactions in solution. *Chem. Commun.* **2017**, *53*, 10902–10905. [[CrossRef](#)]

20. Chu, A.; Hau, F.K.W.; Yao, L.Y.; Yam, V.W.W. Synthesis, structural characterization, and photophysical studies of hexanuclear gold(I) chalcogenido complexes. *J. Chin. Chem. Soc.* **2019**, *66*, 1100–1104. [[CrossRef](#)]
21. Liu, C.Y.; Wei, X.R.; Chen, Y.; Wang, H.F.; Ge, J.F.; Xu, Y.J.; Ren, Z.G.; Braunstein, P.; Lang, J.P. Tetradecanuclear and Octadecanuclear Gold(I) Sulfido Clusters: Synthesis, Structures, and Luminescent Selective Tracking of Lysosomes in Living Cells. *Inorg. Chem.* **2019**. [[CrossRef](#)] [[PubMed](#)]
22. Niermeier, P.; Wickemeyer, L.; Neumann, B.; Stammler, H.G.; Goett-Zink, L.; Kottke, T.; Mitzel, N.W. Auophilicity in action: Stepwise formation of dinuclear Au(i) macrocycles with rigid 1,8-dialkynylanthracenes. *Dalt. Trans.* **2019**, *48*, 4109–4113. [[CrossRef](#)]
23. Beto, C.C.; Zeman, C.J.; Yang, Y.; Bullock, J.D.; Holt, E.D.; Kane, A.Q.; Makal, T.A.; Yang, X.; Ghiviriga, I.; Schanze, K.S.; et al. An Application Exploiting Auophilic Bonding and iClick to Produce White Light Emitting Materials. *Inorg. Chem.* **2020**, *59*, 1893–1904. [[CrossRef](#)] [[PubMed](#)]
24. Alam, P.; Climent, C.; Alemany, P.; Laskar, I.R. “Aggregation-induced emission” of transition metal compounds: Design, mechanistic insights, and applications. *J. Photochem. Photobiol. C Photochem. Rev.* **2019**, *41*, 100317. [[CrossRef](#)]
25. Mei, J.; Leung, N.L.C.; Kwok, R.T.K.; Lam, J.W.Y.; Tang, B.Z. Aggregation-Induced Emission: Together We Shine, United We Soar! *Chem. Rev.* **2015**, *115*, 11718–11940. [[CrossRef](#)]
26. Chen, Z.; Han, X.; Zhang, J.; Wu, D.; Yu, G.A.; Yin, J.; Liu, S.H. Fluorene-based novel gold(i) complexes with aggregation-induced emission (AIE) or aggregate fluorescence change characteristics: From green to white emission. *RSC Adv.* **2015**, *5*, 15341–15349. [[CrossRef](#)]
27. Chen, Z.; Wu, D.; Han, X.; Liang, J.; Yin, J.; Yu, G.A.; Liu, S.H. A novel fluorene-based gold(i) complex with aggregate fluorescence change: A single-component white light-emitting luminophor. *Chem. Commun.* **2014**, *50*, 11033–11035. [[CrossRef](#)]
28. Chen, Z.; Zhang, J.; Song, M.; Yin, J.; Yu, G.A.; Liu, S.H. A novel fluorene-based aggregation-induced emission (AIE)-active gold(i) complex with crystallization-induced emission enhancement (CIEE) and reversible mechanochromism characteristics. *Chem. Commun.* **2015**, *51*, 326–329. [[CrossRef](#)]
29. Chen, Z.; Nie, Y.; Liu, S.H. Fluorene-based mononuclear gold(i) complexes: The effect of alkyl chain, aggregation-induced emission (AIE) and mechanochromism characteristics. *RSC Adv.* **2016**, *6*, 73933–73938. [[CrossRef](#)]
30. Chen, Z.; Yang, L.; Hu, Y.; Wu, D.; Yin, J.; Yu, G.A.; Liu, S.H. Carbazole-based gold(i) complexes with alkyl chains of different lengths: Tunable solid-state fluorescence, aggregation-induced emission (AIE), and reversible mechanochromism characteristics. *RSC Adv.* **2015**, *5*, 93757–93764. [[CrossRef](#)]
31. Chen, Z.; Li, Z.; Hu, F.; Yu, G.A.; Yin, J.; Liu, S.H. Novel carbazole-based aggregation-induced emission-active gold(I) complexes with various mechanofluorochromic behaviors. *Dye. Pigment.* **2016**, *125*, 169–178. [[CrossRef](#)]
32. Gavara, R.; Lima, J.C.; Rodríguez, L. Effect of solvent polarity on the spectroscopic properties of an alkynyl gold(i) gelator. the particular case of water. *Photochem. Photobiol. Sci.* **2016**, *15*, 635–643. [[CrossRef](#)] [[PubMed](#)]
33. Chen, Z.; Liu, G.; Pu, S.; Liu, S.H. Carbazole-based aggregation-induced emission (AIE)-active gold(I) complex: Persistent room-temperature phosphorescence, reversible mechanochromism and vapochromism characteristics. *Dye. Pigment.* **2017**, *143*, 409–415. [[CrossRef](#)]
34. Han, X.; Lü, X.; Chen, Z.; Yu, G.; Yin, J.; Liu, S. A Fluorescent Probe for Hg<sup>2+</sup> Based on Gold(I) Complex with An Aggregation-Induced Emission Feature. *Chin. J. Chem.* **2015**, *33*, 1064–1068. [[CrossRef](#)]
35. Chen, Z.; Li, Z.; Yang, L.; Liang, J.; Yin, J.; Yu, G.A.; Liu, S.H. Novel diisocyno-based dinuclear gold(I) complexes with aggregation-induced emission and mechanochromism characteristics. *Dye. Pigment.* **2015**, *121*, 170–177. [[CrossRef](#)]
36. Chen, Z.; Huang, P.S.; Li, Z.; Yin, J.; Yu, G.A.; Liu, S.H. Triisocyno-based trinuclear gold(I) complexes with aggregation-induced emission (AIE) and mechanochromic luminescence characteristics. *Inorg. Chim. Acta* **2015**, *432*, 192–197. [[CrossRef](#)]
37. Li, W.B.; Luo, W.J.; Li, K.X.; Yuan, W.Z.; Zhang, Y.M. Aggregation-induced phosphorescence and mechanochromic luminescence of a tetraphenylethene-based gold(I) isocyanide complex. *Chin. Chem. Lett.* **2017**, *28*, 1300–1305. [[CrossRef](#)]
38. Wang, X.Y.; Zhang, J.; Dong, Y.B.; Zhang, Y.; Yin, J.; Liu, S.H. Different structures modulated mechanochromism and aggregation-induced emission in a series of Gold(I) complexes. *Dye. Pigment.* **2018**, *156*, 74–81. [[CrossRef](#)]
39. Yang, X.; Wang, S.; Ghiviriga, I.; Abboud, K.A.; Veige, A.S. Organogold oligomers: Exploiting iClick and auophilic cluster formation to prepare solution stable Au<sup>4</sup> repeating units. *Dalt. Trans.* **2015**, *44*, 11437–11443. [[CrossRef](#)]
40. Yang, L.; Cao, Y.; Chen, J.; Sun, Z.; Yao, T.; Jiang, Y.; Wei, S. Luminescence of Au(I)-thiolate complex affected by solvent. *Radiat. Phys. Chem.* **2017**, *137*, 68–71. [[CrossRef](#)]
41. Leung, F.C.M.; Yam, V.W.W. Cation- and Solvent-Induced Supramolecular Aggregation Studies of Crown Ether-Containing Dinuclear Alkynylgold(I) Isocyanide Complexes. *Eur. J. Inorg. Chem.* **2017**, *2017*, 5271–5278. [[CrossRef](#)]
42. Han, Z.; Zhao, X.; Peng, P.; Li, S.; Zhang, C.; Cao, M.; Li, K.; Wang, Z.Y.; Zang, S.Q. Intercluster auophilicity-driven aggregation lighting circularly polarized luminescence of chiral gold clusters. *Nano Res.* **2020**, *13*, 3248–3252. [[CrossRef](#)]
43. Gavara, R.; Llorca, J.; Lima, J.C.; Laura, R. A luminescent hydrogel based on a new au(i) complex. *Chem. Commun.* **2013**, *49*, 72–74. [[CrossRef](#)] [[PubMed](#)]
44. Aguiló, E.; Gavara, R.; Lima, J.C.; Llorca, J.; Rodríguez, L. From Au(i) organometallic hydrogels to well-defined Au(0) nanoparticles. *J. Mater. Chem. C* **2013**, *1*, 5538–5547. [[CrossRef](#)]
45. Gavara, R.; Aguiló, E.; Guerra, C.F.; Rodríguez, L.; Lima, J.C. Thermodynamic aspects of auophilic hydrogelators. *Inorg. Chem.* **2015**, *54*, 5195–5203. [[CrossRef](#)] [[PubMed](#)]

46. Moro, A.J.; Rome, B.; Aguiló, E.; Arcau, J.; Puttreddy, R.; Rissanen, K.; Lima, J.C.; Rodríguez, L. A coumarin based gold(i)-alkynyl complex: A new class of supramolecular hydrogelators. *Org. Biomol. Chem.* **2015**, *13*, 2026–2033. [[CrossRef](#)] [[PubMed](#)]
47. Kemper, B.; Hristova, Y.R.; Tacke, S.; Stegemann, L.; Van Bezouwen, L.S.; Stuart, M.C.A.; Klingauf, J.; Strassert, C.A.; Besenius, P. Facile synthesis of a peptidic Au(i)-metalloamphiphile and its self-assembly into luminescent micelles in water. *Chem. Commun.* **2015**, *51*, 5253–5256. [[CrossRef](#)]
48. Aguiló, E.; Gavara, R.; Baucells, C.; Guitart, M.; Lima, J.C.; Llorca, J.; Rodríguez, L. Tuning supramolecular aurophilic structures: The effect of counterion, positive charge and solvent. *Dalt. Trans.* **2016**, *45*, 7328–7339. [[CrossRef](#)]
49. Gavara, R.; Aguiló, E.; Schur, J.; Llorca, J.; Ott, I.; Rodríguez, L. Study of the effect of the chromophore and nuclearity on the aggregation and potential biological activity of gold(I) alkynyl complexes. *Inorg. Chim. Acta* **2016**, *446*, 189–197. [[CrossRef](#)]
50. Aguiló, E.; Moro, A.J.; Gavara, R.; Alfonso, I.; Pérez, Y.; Zaccaria, F.; Guerra, C.F.; Malfois, M.; Baucells, C.; Ferrer, M.; et al. Reversible Self-Assembly of Water-Soluble Gold(I) Complexes. *Inorg. Chem.* **2018**, *57*, 1017–1028. [[CrossRef](#)]
51. Chu, A.; Hau, F.K.W.; Yam, V.W.W. AuI⋯AuI Interaction Assisted Host–Guest Interactions and Stimuli-Responsive Self-Assembly in Tetranuclear Alkynylgold(I) Calix[4]arene-Based Isocyanide Complexes. *Chem. Eur. J.* **2017**, *23*, 11076–11084. [[CrossRef](#)]
52. Chen, J.; Zhang, Z.; Wang, C.; Gao, Z.; Gao, Z.; Wang, F. Cooperative self-assembly and gelation of organogold(i) complexes: Via hydrogen bonding and aurophilic Au⋯Au interactions. *Chem. Commun.* **2017**, *53*, 11552–11555. [[CrossRef](#)]
53. Zhou, N.; Hailes, R.; Zhang, Y.; Chen, Z.; Manners, I.; He, X. Controlling the supramolecular polymerization of dinuclear isocyanide gold(i) arylethynylene complexes through tuning the central  $\pi$ -conjugated moiety. *Polym. Chem.* **2020**, *11*, 2700–2707. [[CrossRef](#)]
54. Blasco, D.; López-De-Luzuriaga, J.M.; Monge, M.; Olmos, M.E.; Pascual, D.; Rodríguez-Castillo, M. Cooperative Au(I)⋯Au(I) Interactions and Hydrogen Bonding as Origin of a Luminescent Adeninate Hydrogel Formed by Ultrathin Molecular Nanowires. *Inorg. Chem.* **2018**, *57*, 3805–3817. [[CrossRef](#)]
55. Chang, H.Y.; Tseng, Y.T.; Yuan, Z.; Chou, H.L.; Chen, C.H.; Hwang, B.J.; Tsai, M.C.; Chang, H.T.; Huang, C.C. The effect of ligand–ligand interactions on the formation of photoluminescent gold nanoclusters embedded in Au(i)-thiolate supramolecules. *Phys. Chem. Chem. Phys.* **2017**, *19*, 12085–12093. [[CrossRef](#)] [[PubMed](#)]
56. Tseng, Y.T.; Chang, H.Y.; Harroun, S.G.; Wu, C.W.; Wei, S.C.; Yuan, Z.; Chou, H.L.; Chen, C.H.; Huang, C.C.; Chang, H.T. Self-Assembled Chiral Gold Supramolecules with Efficient Laser Absorption for Enantiospecific Recognition of Carnitine. *Anal. Chem.* **2018**, *90*, 7283–7291. [[CrossRef](#)]
57. Wu, Z.; Du, Y.; Liu, J.; Yao, Q.; Chen, T.; Cao, Y.; Zhang, H.; Xie, J. Aurophilic Interactions in the Self-Assembly of Gold Nanoclusters into Nanoribbons with Enhanced Luminescence. *Angew. Chem. Int. Ed.* **2019**, *58*, 8139–8144. [[CrossRef](#)]
58. Yam, V.W.W.; Li, C.K.; Chan, C.L. Proof of potassium ions by luminescence signaling based on weak gold–Gold interactions in dinuclear gold(I) complexes. *Angew. Chem. Int. Ed.* **1998**, *37*, 2857–2859. [[CrossRef](#)]
59. Leung, F.C.M.; Yam, V.W.W. Photophysical and ion-binding studies of a tetranuclear alkynylgold(I) isonitrile complex. *J. Photochem. Photobiol. A Chem.* **2018**, *355*, 212–219. [[CrossRef](#)]
60. Guo, Y.; Tong, X.; Ji, L.; Wang, Z.; Wang, H.; Hu, J.; Pei, R. Visual detection of  $\text{Ca}^{2+}$  based on aggregation-induced emission of Au(i)-Cys complexes with superb selectivity. *Chem. Commun.* **2015**, *51*, 596–598. [[CrossRef](#)] [[PubMed](#)]
61. Wakabayashi, R.; Maeba, J.; Nozaki, K.; Iwamura, M. Considerable enhancement of emission yields of  $[\text{Au}(\text{CN})_2]^-$  oligomers in aqueous solutions by coexisting cations. *Inorg. Chem.* **2016**, *55*, 7739–7746. [[CrossRef](#)]
62. Toohara, S.; Tanaka, Y.; Sakurai, S.; Ikeda, T.; Tanaka, K.; Gon, M.; Chujo, Y.; Kuroiwa, K. Self-assembly of  $[\text{Au}(\text{CN})_2]^-$  complexes with tomato (*Solanum lycopersicum*) steroidal alkaloid glycosides to form sheet or tubular structures. *Chem. Lett.* **2018**, *47*, 1010–1013. [[CrossRef](#)]
63. Zheng, L.; Ye, X.; Qi, P.; Zhang, D.; Sun, Y. Fluorometric detection of sulfate-reducing bacteria via the aggregation-induced emission of glutathione-gold(I) complexes. *Microchim. Acta* **2019**, *186*, 1–8. [[CrossRef](#)] [[PubMed](#)]
64. Pinto, A.; Spigolon, G.; Gavara, R.; Zonta, C.; Licini, G.; Rodríguez, L. Tripodal gold(i) polypyridyl complexes and their Cu+ and Zn2+ heterometallic derivatives. Effects on luminescence. *Dalt. Trans.* **2020**, *49*, 14613–14625. [[CrossRef](#)]
65. Giestas, L.; Gavara, R.; Aguiló, E.; Svahn, N.; Lima, J.C.; Rodríguez, L. Modulation of supramolecular gold(I) aggregates by anion's interaction. *Supramol. Chem.* **2018**, *30*, 278–285. [[CrossRef](#)]
66. Moro, A.J.; Avó, J.; Malfois, M.; Zaccaria, F.; Fonseca Guerra, C.; Caparrós, F.J.; Rodríguez, L.; Lima, J.C. Aggregation induced emission of a new naphthyridine-ethynyl-gold(i) complex as a potential tool for sensing guanosine nucleotides in aqueous media. *Dalt. Trans.* **2020**, *49*, 171–178. [[CrossRef](#)]
67. Guo, P.; He, Q.; Wang, C.; Hou, Z.; Yu, B.; Bu, W. Intensely phosphorescent block copolymer micelles containing gold(I) complexes. *Soft Matter* **2018**, *14*, 3521–3527. [[CrossRef](#)] [[PubMed](#)]
68. Guo, P.; Jin, R.; Wang, M.; He, Q.; Cai, C.; Zhao, Q.; Bu, W. Chiral gold(I)-containing polymeric composites: Chiroptical sensing and circularly polarized luminescence. *J. Organomet. Chem.* **2021**, *931*, 121616. [[CrossRef](#)]
69. Zhang, J.; Liu, Q.; Wu, W.; Peng, J.; Zhang, H.; Song, F.; He, B.; Wang, X.; Sung, H.H.Y.; Chen, M.; et al. Real-Time Monitoring of Hierarchical Self-Assembly and Induction of Circularly Polarized Luminescence from Achiral Luminogens. *ACS Nano* **2019**, *13*, 3618–3628. [[CrossRef](#)] [[PubMed](#)]